

A Survey on 3D Gaussian Splatting Applications: Segmentation, Editing, and Generation

Shuting He, Peilin Ji, Yitong Yang, Changshuo Wang, Jiayi Ji, Yinglin Wang, Henghui Ding

Abstract—3D Gaussian Splatting (3DGS) has recently emerged as a powerful alternative to Neural Radiance Fields (NeRF) for 3D scene representation, offering high-fidelity photorealistic rendering with real-time performance. Beyond novel view synthesis, the explicit and compact nature of 3DGS enables a wide range of downstream applications that require geometric and semantic understanding. This survey provides a comprehensive overview of recent progress in 3DGS applications. It first introduces 2D foundation models that support semantic understanding and control in 3DGS applications, followed by a review of NeRF-based methods that inform their 3DGS counterparts. We then categorize 3DGS applications into segmentation, editing, generation, and other functional tasks. For each, we summarize representative methods, supervision strategies, and learning paradigms, highlighting shared design principles and emerging trends. Commonly used datasets and evaluation protocols are also summarized, along with comparative analyses of recent methods across public benchmarks. To support ongoing research and development, a continually updated repository of papers, code, and resources is maintained at <https://github.com/heshuting555/Awesome-3DGS-Applications>.

Index Terms—Survey, 3D Gaussian Splatting, Application, Segmentation, Editing, Generation

1 INTRODUCTION

3D Gaussian Splatting (3DGS) [1] has recently emerged as a powerful paradigm for real-time neural rendering, achieving high-fidelity photorealistic synthesis with superior efficiency. Unlike implicit field-based methods such as Neural Radiance Fields (NeRFs) [2], which rely on volumetric integration over coordinate-based neural networks, 3DGS represents scenes as explicit collections of anisotropic 3D Gaussians and renders them via differentiable rasterization. This explicit yet learnable formulation enables efficient optimization and fast inference, while preserving fine-grained geometric and appearance details. As a next-generation neural representation, 3DGS has demonstrated remarkable potential across a broad spectrum of applications, including virtual and augmented reality, robotics, autonomous navigation, and urban mapping.

While early research on 3DGS [1], [3], [4] primarily focused on novel view synthesis, recent works have extended its scope to a growing number of downstream tasks, such as simultaneous localization and mapping (SLAM) [5], human avatar [6], segmentation [7], editing [8], generation [9], and more. These applications require richer representations that go beyond geometry to incorporate semantics, spatial relationships, and multi-modal cues. Compared to NeRF-based frameworks, 3DGS offers a more structured and interpretable formulation that enables efficient optimization, direct supervision, and intuitive manipulation. These properties make it advantageous for high-level tasks beyond rendering.

Although several recent surveys [10], [11], [12], [13] have documented the rapid development of 3DGS, they primarily focus on global taxonomies, real-time rendering pipelines, or compression strategies, while offering limited insights into 3DGS-driven

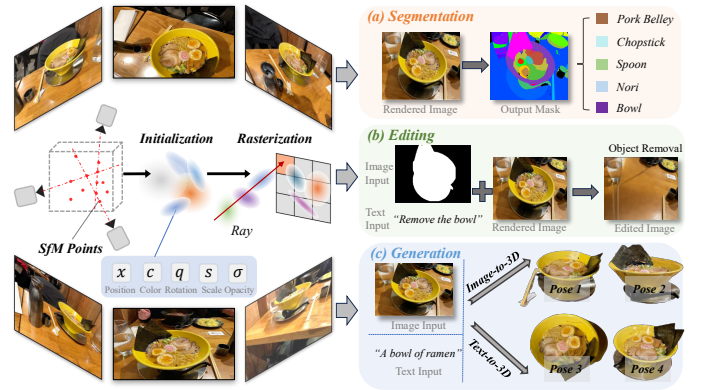


Fig. 1: Overview of the three main 3DGS applications. (a) *Segmentation*: Segment each semantic region. (b) *Editing*: Perform editing via text or image prompt. (c) *Generation*: Support text-to-3D and image-to-3D generation.

downstream applications. A few works [14], [15], [16] attempt to cover application domains, but typically lack systematic analysis of underlying design principles, methodological innovations, or benchmarking protocols. To address this gap, we present the first dedicated survey that systematically reviews downstream applications of 3DGS beyond classical view synthesis. Specifically, we focus on three rapidly evolving directions, namely segmentation, editing, and generation, as illustrated in Fig. 1.

• **Contribution.** This survey provides a comprehensive and structured review of recent literature on 3DGS with a focus on its emerging downstream applications. We begin by introducing 2D foundation models that enable semantic control and understanding in 3DGS-based systems, and briefly revisit relevant NeRF-based methods to establish conceptual continuity. The core of our survey is organized around three major task categories: segmentation, editing, and generation. Within each category, we systematically compare representative works in terms of technical designs, learn-

- S. He, P. Ji, Y. Yang, and Y. Wang are with Shanghai University of Finance and Economics, China. shuting.he@sufe.edu.cn.
- C. Wang is with University College London, United Kingdom.
- J. Ji is with National University of Singapore, Singapore.
- H. Ding is with Fudan University, China. henghui.ding@gmail.com.

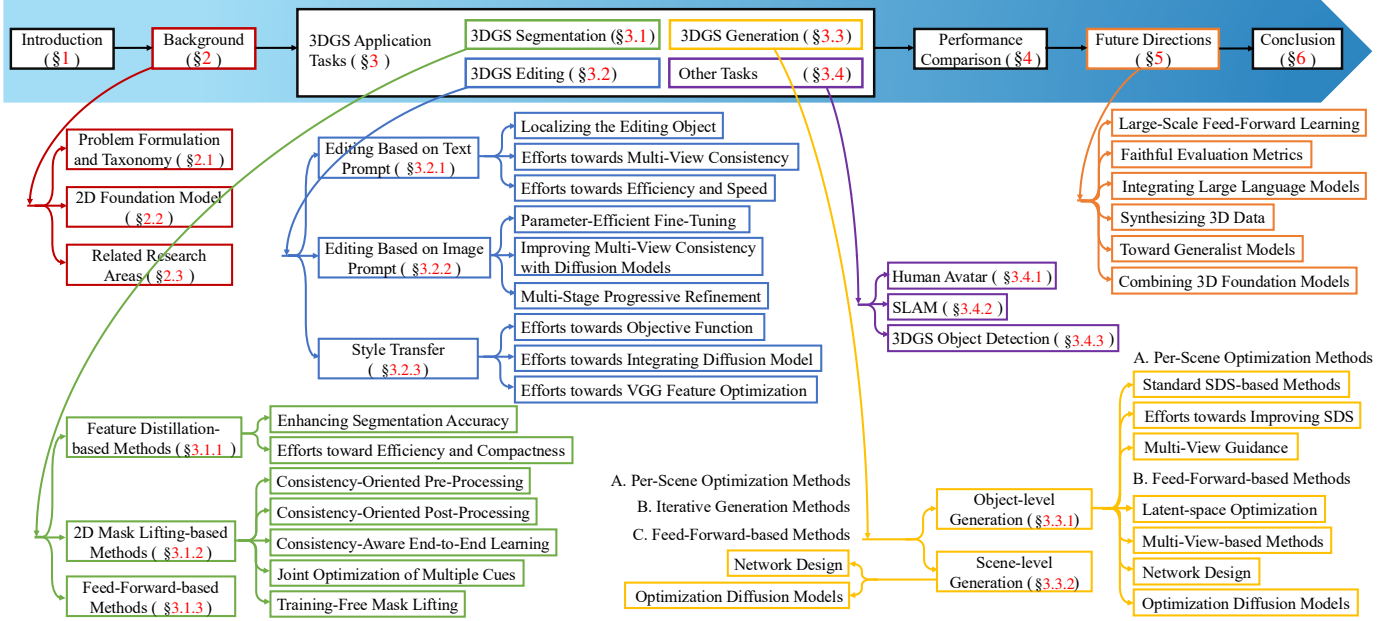


Fig. 2: An overview diagram illustrating the structure of this survey.

ing paradigms, and supervision strategies. We further analyze benchmark settings and performance results in each domain, aiming to provide a self-contained and accessible resource for both newcomers and experienced researchers. Finally, we discuss open challenges and future research opportunities, with the goal of fostering deeper exploration and broader adoption of 3DGS across high-level vision and graphics application tasks.

• **Organization.** Fig. 2 provides an overview of the structure of this survey. In Sec. 2, we introduce essential background knowledge, including key definitions, commonly used 2D foundation models, and relevant NeRF-based research that informs 3DGS development. Sec. 3 presents a task-centric review of recent 3DGS-based methods, with a focus on segmentation, editing, and generation. In Sec. 4, we summarize evaluation protocols and benchmark settings, and provides quantitative comparisons across tasks and datasets to assess the performance of existing approaches. Sec. 5 discusses open challenges and outlines potential future research directions. Finally, Sec. 6 concludes the survey with a summary of key insights and takeaways.

2 BACKGROUND

In this section, we first categorize the main research directions of 3DGS for downstream applications. We then provide a concise overview of widely used 2D foundation models that support these tasks. Finally, we review related research domains in the NeRF literature that lay the groundwork for 3DGS development.

2.1 Problem Formulation and Taxonomy

Let \mathcal{X} and \mathcal{Y} denote the input and output spaces, respectively. In the context of 3DGS-based downstream applications, the objective is to learn an ideal mapping function $f^*: \mathcal{X} \mapsto \mathcal{Y}$ that transforms visual observations into task-specific outputs such as semantic understanding, controllable editing, or content generation. Specifically, given a set of posed RGB images $\{x_n^s\}_{n,s} \subset \mathcal{X}$, where n denotes the number of views, s represents different scenes, 3DGS provides a differentiable intermediate representation that bridges perception and application-level tasks.

2.1.1 Application Tasks Category

Depending on the nature of the output space \mathcal{Y} , downstream applications built upon 3DGS can be broadly categorized into three representative directions: segmentation, editing, and generation.

• **3DGS Segmentation.** Based on the input space \mathcal{X} , existing 3DGS segmentation methods can be broadly classified into two categories: generic segmentation and promptable segmentation. Generic segmentation aims to predict pixel- or point-level labels without external prompts, and can be further divided into: (i) Semantic segmentation [17]; (ii) Instance segmentation [18], [19], [20]; and (iii) Panoptic segmentation [21], [22]. Promptable segmentation extends the generic setting by introducing external prompts to guide the segmentation process. Depending on the form of prompts, this category includes: (i) Interactive segmentation, where users provide spatial hints such as clicks, scribbles, boxes, or masks [23], [24], [25]; (ii) Open-vocabulary segmentation, which uses category names as textual prompts to support segmenting novel or unseen classes [26], [27]; (iii) Referring segmentation, which relies on natural language expressions to localize and segment specific objects [7]. In addition, depending on the representation of the output space \mathcal{Y} , segmentation results can be produced either on rendered 2D images [26], [28] or directly over the 3D Gaussian representations [29], [30], [31], [32].

• **3DGS Editing.** Editing tasks aim to modify scene attributes such as geometry, appearance, or illumination, while maintaining structural and visual consistency across viewpoints. In this setting, \mathcal{Y} denotes the edited scene state, often represented by an updated set of Gaussians. 3DGS facilitates localized and differentiable editing operations, including addition, deletion, and transformation of scene components, thus enabling applications such as content-aware inpainting and style-consistent relighting. Based on the form of inputs \mathcal{X} , editing approaches can be categorized into image-guided [33], [34] and text-guided methods [8], [35], [36].

• **3DGS Generation.** Generation involves synthesizing novel 3D scenes or objects from limited inputs such as a single image, a sparse set of views, or a textual prompt. Here, \mathcal{Y} represents the desired 3D output in the form of Gaussian primitives. Recent approaches enable direct generation of structured 3D content,

supporting high-quality synthesis and compositionality within multimodal AIGC frameworks. Depending on the modality of inputs, generation methods can be grouped into image-to-3D [37], [38], [39] and text-to-3D paradigms [40], [41], [42]. Alternatively, generation methods can be categorized by output granularity into object-level [9], [40] and scene-level generation [43], [44].

2.1.2 Learning Paradigms for Application Tasks

- **Per-scene Optimization.** In this paradigm, the model learns a scene-specific mapping f_{θ_s} for each individual scene s , where θ_s denotes parameters optimized solely for that scene. Given multi-view observations $\{x_n^s\}_n$ for one scene, the objective is to minimize a reconstruction loss across views:

$$\tilde{\theta}_s \in \arg \min_{\theta_s} \frac{1}{N} \sum_n \varepsilon(f_{\theta_s}(x_n^s), x_n^s), \quad (1)$$

where $\varepsilon(\cdot, \cdot)$ denotes a task-specific reconstruction loss function, such as an ℓ_1 loss, depending on the target application. This per-scene fitting scheme enables high-fidelity modeling tailored to each scene, making it well-suited for tasks requiring view-consistent reconstruction or dense appearance modeling. However, the lack of generalization and high computational cost make it impractical for large-scale or real-time applications.

- **Feed-forward Learning.** This alternative seeks to approximate a universal function f_θ that generalizes across scenes. A shared parameter set θ is learned from a collection of scenes $\{x_n^s\}_{n,s} \subset \mathcal{X}$ drawn from diverse environments:

$$\tilde{\theta} \in \arg \min_{\theta} \frac{1}{NS} \sum_{n,s} \varepsilon(f_\theta(x_n^s), x_n^s). \quad (2)$$

The learned function f_θ allows direct inference on novel scenes via a single forward pass, supporting efficient generation and scalable deployment. While typically less precise than per-scene methods in modeling fine-grained geometry or photometric details, feed-forward approaches offer strong potential for real-time applications and serve as a foundation for generalizable 3D perception.

2.2 2D Foundation Model

The success of 3DGS applications relies heavily on the integration of powerful 2D foundation models. Given the limited availability of large-scale 3D datasets, learning robust 3D representations remains challenging. To address this, a number of methods leverage pretrained 2D priors to enhance 3D representation.

- **Foundation Features for Vision Tasks (DINO&DINOv2).** DINO [45] frames self-supervised ViT training as self-distillation without labels, where the model learns from its own predictions. Despite its moderate size, it yields semantically rich features effective for object understanding. DINOv2 [46] scales this approach with larger models, more data, and refined training, producing strong general-purpose features competitive with supervised baselines. These models reveal emergent capabilities in part-level reasoning and robust representations, making them valuable.

- **Contrastive Language-Image Pre-training (CLIP).** CLIP [47] trains separate image and text encoders on 400M web pairs, using a contrastive loss that brings matched embeddings together in a shared space while pushing mismatches apart. The resulting representation carries broad semantic knowledge and strong zero-shot ability, making CLIP a standard backbone for open-vocabulary and multimodal tasks.

- **Segment Anything (SAM).** SAM [48] is a foundation model for image segmentation, trained on 1B masks over 11M images

using a promptable paradigm. It supports versatile inputs—points, boxes, masks, or text—and enables zero-shot generalization across diverse segmentation tasks. While powerful, its heavy vision backbone limits efficiency, SAM2 [49] mitigates this with a hierarchical encoder, achieving real-time performance and improved accuracy in the video domain [50], [51], [52], [53].

- **Diffusion Models (DMs).** These generative models start from Gaussian noise and progressively denoise it, step-by-step, into a coherent image; the denoiser is trained to invert a fixed noise schedule (DDPM [54]). Latent diffusion (LDM [55]) performs the same procedure in the auto-encoder’s latent space, making high-resolution synthesis tractable on everyday GPUs. Text-conditioned variants, *e.g.*, Stable Diffusion [55], inject cross-attention to a language encoder, allowing precise, prompt-driven control while preserving visual fidelity. Their attention maps have been shown to correlate with meaningful regions in the output, connecting image generation with vision–language understanding.

2.3 Related Research Areas

- **Segmentation Based on NeRF.** Semantic NeRF [56] pioneers the incorporation of semantic information into radiance fields by introducing per-point semantic layers. Follow-up works can be broadly categorized into two directions. The first focuses on feature distillation, where high-dimensional 2D features from pretrained vision models (*e.g.*, DINO, CLIP) are embedded into 3D neural fields. Representative methods such as Distilled Feature Fields [57], Neural Feature Fusion Fields [58], ISRF [59], LERF [60], and 3D-OVS [61] optimize volumetric feature fields to reconstruct semantic features via differentiable rendering. The second line of research targets mask lifting, which seeks to overcome the scarcity of 3D annotations by projecting 2D semantic masks into 3D space. Early methods rely on either ground-truth masks [62], [63] or pretrained segmentation models, such as methods like Panoptic Lifting [64], ContrastiveLift [65], and SPIn-NeRF [66]. However, these approaches often suffer from limited generalization due to closed-set assumptions. With the recent emergence of powerful foundation models like SAM and SAM2 [48], newer works aim to leverage their open-world segmentation capabilities. For instance, SA3D [67] proposes an interactive pipeline that propagates a single SAM mask across multiple views into a NeRF-based scene, enabling sparse-to-dense segmentation. GARField [68] further explores integrating SAM-derived cues into radiance field optimization.

- **Editing Based on NeRF.** Recent progress in NeRF-based editing and manipulation has led to more intuitive and controllable frameworks for modifying 3D scenes and objects. Early efforts introduce conditional radiance fields that support localized editing through sparse 2D user inputs, enabling view-consistent changes in appearance and shape with minimal supervision [69]. Building on this, CLIP-NeRF [70] pioneers text- and image-driven NeRF editing using disentangled latent spaces for geometry and appearance, allowing independent control guided by CLIP embeddings and supporting both category-level generation and real image inversion. Subsequent methods have addressed object-level editing and inpainting. Object-NeRF [71] and LaTeRF [72] further explore object-centric manipulation and structural completion in NeRF scenes. CoNeRF [73] introduces fine-grained, attribute-specific control with few-shot supervision, leveraging sparse 2D mask annotations and a quasi-conditional latent structure to enable localized edits and novel expression synthesis. Unified models

that combine segmentation with NeRF-based inpainting further enable intuitive scene manipulation, such as object removal and completion from sparse cues [66]. Instruct-NeRF2NeRF [74] employs an image-conditioned diffusion model to iteratively edit input images while jointly optimizing the underlying 3D scene.

- **Generation Based on NeRF.** NeRF-based generative models have rapidly advanced 3D-aware content synthesis. Early works utilize implicit volumetric representations with adversarial training to achieve 3D consistent image generation from unposed views, improving shape–appearance disentanglement and scalability [75]. To boost efficiency and detail, later methods constrain sampling to 2D manifolds via ray-surface intersections [76]. A major shift occurs with Score Distillation Sampling (SDS), which enables NeRF optimization from text prompts using 2D diffusion models, eliminating the need for 3D supervision [77]. Follow-up work adopts coarse-to-fine strategies and hybrid representations to enhance quality and speed [78]. Latent-NeRF [79] uses Sketch-Shape to define the coarse structure of abstract geometric objects, enabling text- and shape-guided control over the generation process. Wang *et al.* [80] apply the chain rule to the learned gradients and backpropagate the diffusion model’s score through the Jacobian of a differentiable renderer, instantiated as a voxel radiance field. In parallel, GAN-based models introduce tri-plane features and pose-aware training to generate high-resolution, multi-view consistent outputs [81]. Recent diffusion-guided approaches further extend to full-scene generation by combining semantic priors and progressive inpainting for photorealistic results [82].

3 3DGS APPLICATION TASKS

3.1 3DGS Segmentation

3DGS segmentation encompasses a broad spectrum of task definitions, as discussed in Sec. 2.1.1. Given the overlapping nature of segmentation tasks and that a single method may apply to multiple scenarios, we organize existing approaches based on their technical characteristics rather than task formulations.

3.1.1 Feature Distillation-based Methods

These methods [26], [27], [83], [84] aim to distill the semantic knowledge embedded in 2D foundation models (*e.g.*, CLIP [47], SAM [48], DINO [45]) into 3D scene representations. By leveraging the semantic understanding learned from large-scale 2D datasets, these approaches enhance 3D models with open-vocabulary recognition capabilities. LangSplat [26] and Feature3DGS [27] are among the earliest works to explore this direction. LangSplat first segments images using SAM [48], and then feeds the resulting hierarchical semantic masks into CLIP to extract region-level semantic embeddings. To alleviate memory constraints, it employs a scene-specific language autoencoder to compress these high-dimensional semantic features. These compressed features are used to supervise a set of initialized 3D Gaussian language features, effectively transferring CLIP’s open-vocabulary semantics into the 3D domain for downstream tasks. Feature3DGS, developed concurrently, distills features from LSeg [85] and SAM [48], and further employs SAM’s decoder to interpret 2D rendered views, establishing a bridge between 2D and 3D segmentation. While effective, these methods may suffer from semantic information loss and high computational cost. To address these limitations, subsequent works have evolved along two key directions: improving segmentation accuracy and reducing computation overhead.

- **Enhancing Segmentation Accuracy.** N2F2 [86] addresses LangSplat’s inefficiency in scale selection by learning a unified high-dimensional feature field under hierarchical supervision, where each feature dimension encodes scene semantics at different granularities, enabling fine-grained yet efficient representation without multi-scale querying. LangSurf [87] improves LangSplat by extracting dense pixel-level semantics from the entire image, followed by SAM-based mask pooling to preserve contextual cues. It also jointly optimizes language Gaussians on object surfaces using geometry supervision and contrastive loss, enhancing object’s spatial consistency in 3D. seconGS [88] further refines LangSplat by using SAM2-generated masklets to provide semantically consistent supervision. To overcome the limitations of 2D querying in 3D space, it introduces a two-step querying mechanism that first retrieves distilled ground-truth and then queries individual Gaussians for spatially accurate 3D understanding. VLGaussian [28] observes that prior color-based rasterization is unsuitable for language modalities due to its dependence on the same color opacity. Instead, it introduces a cross-modal rasterizer tailored for rendering semantic language features with newly introduced opacity for language. SuperGSeg [89], inspired by superpoint representations, clusters Gaussians into Super-Gaussians using spatial and instance cues based on Scaffold-GS [3]. High-dimensional language features are assigned to each Super-Gaussian to support structured and comprehensive scene understanding while preserving linguistic granularity. Unlike existing methods that distill 2D knowledge to 3D projected view, SemanticGaussians [90] design a versatile projection approach that maps various 2D semantic features from pre-trained image encoders into a semantic component of 3D Gaussians based on spatial relationships. It distills projected 2D knowledge into 3D semantic network directly for fast inference. Beyond the aforementioned approaches that solely introduce semantic information, GLS [91] incorporates geometric priors (surface normals) to effectively refine the rendered depth.

- **Efforts toward Efficiency and Compactness.** To mitigate the substantial memory overhead incurred by increasing feature channels in raw semantic features, LEGaussian [83] quantizes dense language features into a discrete feature space and semantic indices, and applies a smoothing loss to retain rendering quality with quantized representation. CLIP-GS [92] introduces semantic attribute compactness to efficiently encode scene semantics with Gaussians, enabling fast training and inference. It further improves 3D segmentation by employing a 3D-coherent self-training strategy that enhances cross-view semantic consistency. Later, FMGS [93] integrates 3D Gaussian scene representation with multi-resolution hash encodings (MHE) to enable efficient semantic embedding. Unlike previous methods, it avoids scene-specific quantization or autoencoders, thereby preserving the semantic fidelity of foundation model features. GOI [94] introduces a trainable feature clustering codebook that compresses high-dimensional, noisy semantic features into compact representations guided by scene priors. It effectively preserves semantic expressiveness while significantly reducing storage and rendering overhead. FastLGS [95] constructs a semantic feature grid that stores multi-view CLIP features extracted from SAM-generated masks. These grid features are then projected into a low-dimensional space and used to supervise semantic field training. Building upon FastLGS, FMLGS [96] enables part-level open-vocabulary queries in 3DGS by constructing consistent object-part semantics via SAM2, and introduces a semantic deviation strategy to enrich fine-grained features, allowing natural language queries over both

objects and their parts. To address the high memory cost of jointly encoding color and semantics in existing 3DGS-based methods [27], [83], [92], DF-3DGS [97] decouples color and semantic fields to reduce Gaussian usage for semantics, and introduces a hierarchical compression pipeline combining dynamic quantization and scene-specific autoencoding for efficient representation. In summary, knowledge distillation provides a practical mechanism to bridge 2D foundation models and 3D Gaussian representations. While early methods focus on direct supervision, recent advances have introduced architectural, supervisory, and efficiency-oriented innovations to improve precision and scalability. These works collectively advance open-vocabulary 3D understanding under constrained computational and data resources.

3.1.2 2D Mask Lifting-based Methods

Accurate 3DGS segmentation remains challenging due to limited annotation and costly labeling. To address this, recent works explore lifting 2D masks from foundation models (*e.g.*, SAM [48], SAM2 [49]) into 3D. However, 2D masks often suffer from cross-view inconsistency, where the same object may receive different instance IDs from different views, as well as quality issues like over- and under-segmentation, making direct lifting non-trivial.

- **Consistency-Oriented Pre-Processing.** Several methods [19], [21], [22], [98], [99], [100] aim to improve multi-view mask consistency through pre-processing strategies before lifting 2D masks into 3D. GaussianGrouping [22] introduces an object association technique as a pre-processing step to align 2D segmentation maps across views, enhancing cross-view consistency. However, the quality of such pre-processing is often limited by errors in object correspondence under varying viewpoints. Gaga [19] addresses this by leveraging spatial cues and a 3D-aware memory bank to effectively associate object masks across diverse camera poses. CCGS [21] further argues that Gaga lacks segmentation-aware optimization within the Gaussian representation itself, which may lead to inconsistent or floating structures in the 3D segmentation field. To overcome this, CCGS constructs a unified 3D point cloud field and performs segmentation-constrained optimization to reinforce mask association through spatial regularization.

- **Consistency-Oriented Post-Processing.** While pre-processing strategies help improve mask alignment across views, they are often susceptible to accumulated errors that degrade segmentation quality. To address this, recent methods [18], [101] have shifted focus to post-processing techniques that refine multi-view predictions after initial lifting. For instance, OmniSeg3D [18] encodes instance-level semantics into a feature field through hierarchical contrastive learning. It then applies a hierarchical clustering algorithm in post-processing to merge and refine the lifted masks, ultimately yielding consistent and coherent 3D instance segmentations across views. Similarly, CAGS [101] leverages instance clustering and semantic matching to associate 3D instances with 2D open-vocabulary priors, thereby enhancing semantic consistency.

- **Consistency-Aware End-to-End Learning.** To reduce reliance on heuristic pre- and post-processing, recent works [17], [24], [30], [32], [102], [103], [104] propose end-to-end learning frameworks that directly construct consistent and distinguishable 3D feature fields. SAGA [30] distills 2D masks into 3D features that introduce a scale-aware contrastive training strategy that distills SAM’s segmentation capability into a scale-gated affinity representation, which handles multi-granularity ambiguity. SA3D [102] introduces an iterative refinement strategy that alternates between inverse rendering of 2D masks and cross-view self-prompting,

enabling progressively more consistent and accurate object segmentation across multiple views. Click-Gaussian [24] enables efficient interactive segmentation of 3D Gaussians by incorporating multi-granularity feature fields derived from 2D masks. It further introduces Global Feature-guided Learning (GFL) to alleviate inconsistencies across different views. Unified-Lift [20] develops an object-aware lifting pipeline that eliminates the need for additional alignment steps. It formulates a codebook-based object representation and aligns object-level semantics with Gaussian features via contrastive learning, leading to improved 3D instance understanding. OpenGaussian [32] focuses on 3D open-vocabulary segmentation by leveraging SAM-predicted masks to supervise 3D instance features. It adopts a coarse-to-fine feature discretization strategy via a two-stage codebook and introduces an instance-level 3D–2D association module that bridges Gaussian points with 2D masks and CLIP embeddings. econSG [105] improves zero-shot 3D semantic understanding by projecting refined multi-view language features into a low-dimensional 3D latent space, enabling efficient optimization and consistent semantic field initialization within the 3D Gaussian framework. CCL-LGS [106] aligns SAM-generated masks across views using a zero-shot tracker and extracts semantic features with CLIP. A contrastive codebook learning module is then applied to enforce cross-view consistency by promoting intra-class compactness and inter-class separation in the learned semantic space. VoteSplat [107] integrates Hough voting with 3DGS by learning a per-Gaussian 3D offset whose projections align with SAM-derived 2D vote maps and are depth-regularized, so that votes aggregate near object centroids. ILGS [108] addresses view-inconsistent language embeddings challenge by introducing two key components: an identity-aware semantic consistency loss that enforces alignment of language features across views, and a progressive mask expansion to enhance boundary precision by modeling local segment relationships.

- **Joint Optimization of Multiple Cues.** To enhance the precision of 2D mask lifting, recent methods jointly optimize semantic, appearance, and geometric cues end-to-end. COB-GS [109] proposes a joint optimization framework that simultaneously learns semantics and texture, leading to sharper object boundaries while preserving visual fidelity. PanoGS [110] formulates a language-guided graph cut mechanism that aggregates 3D Gaussian primitives into super-primitives by leveraging both reconstructed geometry and linguistic signals. It further applies graph-based clustering with SAM-guided edge affinity to produce 3D-consistent panoptic segmentations. InstanceGaussian [31] mitigates the mismatch between appearance and semantics by progressively co-training both modalities within the Scaffold-GS [3] framework, achieving better alignment and instance-level coherence.

- **Training-Free Mask Lifting.** To avoid the computational cost and data requirements of model training, several methods explore training-free strategies that directly associate 2D segmentation masks with 3D Gaussian primitives for efficient 3D segmentation. SAGD [23] adopts a simple yet effective projection-based strategy: the centers of 3D Gaussians are projected onto 2D masks, and those falling within foreground regions are classified as foreground Gaussians. FlashSplat [111] formulates the mask lifting process as a one-step linear programming (LP) optimization problem, directly transforming 2D mask supervision into 3D Gaussian masks without iterative training. GaussianCut [29] represents the scene as a graph over Gaussians and applies graph-cut optimization to partition them into foreground and background. It leverages coarse segmentation from 2D image/video models and refines the

results through learned edge affinities in the constructed graph. THGS [112] constructs a hierarchical superpoint graph from 3D Gaussian primitives and reprojects 2D semantic features onto this structure, producing a view-consistent semantic field without the need for supervised training. iSegMan [25] introduces a visibility-guided voting scheme that links 2D segmentations from SAM with 3D Gaussians, treating the association as a voting process weighted by Gaussian visibility. LBG [113] assigns semantics to 3D Gaussians via a 2D-to-3D lifting and incrementally merges them based on semantic and geometric overlap, enabling fast training-free 3D instance segmentation. LUDVIG [114] introduces “inverse rendering” aggregation, where 2D features or masks from multiple views are uplifted to the 3D by performing a weighted average guided by the 3DGS rendering weights. Then, a graph diffusion mechanism is designed for feature refinement.

3.1.3 Feed-Forward-based Methods

To overcome the inefficiency of per-scene optimization, especially under dense calibrated images conditions, several methods [115], [116], [117], [118], [119] adopt feed-forward architectures to enable fast and generalizable 3D semantic field construction. SLGaussian [115] builds a feed-forward pipeline that infers 3D semantic Gaussians directly from sparse viewpoints based on MVSPlat [4]. It enforces mask consistency via video-based tracking and embeds language features by indexing high-dimensional CLIP representations through compact low-dimensional codes, achieving efficient and scalable 3D understanding. Dr. Splat [117] departs from traditional rendering-based supervision by directly associating CLIP embeddings with 3D Gaussians. It introduces a language feature registration mechanism that assigns CLIP features to dominant Gaussians intersected by pixel rays. Additionally, it employs Product Quantization (PQ) learned from large-scale image datasets to compress features. LangScene-X [119] first uses a TriMap video diffusion network based on CogVideoX [120] to densify sparse inputs, synthesizing appearance, geometry, and semantics. It then employs a Language-Quantized Compressor (LQC) to encode language embeddings on large-scale datasets. SceneSplat [121] introduces a self-supervised framework that facilitates rich 3D feature learning from unlabeled scenes. To support this effort, SceneSplat-7K is introduced as the first large-scale dataset specifically designed for 3DGS in indoor environments.

3.2 3DGS Editing

Inspired by 2D editing methods [122], [123], editing works based on 3D Gaussian Splatting (3DGS) have advanced. These methods leverage the rich scene representation of 3DGS and often incorporate 2D diffusion models to guide precise 3D modifications. This section reviews and categorizes editing techniques and tasks.

3.2.1 Editing Based on Text Prompt

Text-Driven 3D Editing [124], [125], [126] represents an emerging and rapidly advancing technology that allows users to enable convenient and efficient editing or generation of 3D scenes through simple natural language instructions, significantly reducing the technical barriers to 3D modeling and content creation.

- **Localizing the Editing Object.** Most current research first requires text to locate the objects that need to be edited. GaussianEditor [8], [35], as pioneering work in the field of 3D editing based on 3D Gaussian Splatting technology, proposes innovative editing methodologies. The former significantly enhances editing

precision by integrating textual descriptions throughout the training process to track editing targets. The latter achieves refined control over the editing process by extracting regions of interest (ROIs) corresponding to textual instructions and mapping these regions to 3D Gaussians. These methods leverage the Instruct-Pix2Pix [122] model during the editing process, but due to its inherent limitations, issues like inaccurate localization and limited editing control still persist. To address these, GSEditPro [127] introduces an attention-based progressive localization module, leveraging cross-attention layers from the T2I model to classify Gaussians and precisely localize editing regions. It also incorporates DreamBooth [128] for enhanced diversity and flexibility. Xiao *et al.* [129] propose a lighting-aware 3D scene editing pipeline, utilizing an Anchor View Proposal (AVP) algorithm to identify target regions and a coarse-to-fine optimization process with Depth-guided Inpainting Score Distillation Sampling (DI-SDS) for texture and lighting consistency.

- **Efforts towards Multi-View Consistency.** Editing 3D objects while maintaining multi-view consistency is a core challenge in the field of 3D editing. GaussCtrl [130] leverages depth-conditioned editing by utilizing naturally consistent depth maps to ensure geometric consistency across multi-view images, along with attention-based latent code alignment to achieve a unified appearance across views. Luo *et al.* [131] propose a progressive 3D editing strategy using a Trajectory-Anchored Scheme (TAS) and a dual-branch editing mechanism to ensure multi-view consistency, addressing challenges in error accumulation during text-to-image processes. Eyal *et al.* [132] introduce a geometry-guided warping mechanism that leverages the scene’s depth and structural information to accurately map edits across views, ensuring multi-view consistency. DGE [133] employs spatiotemporal attention to jointly edit the selected key views and inject their features into other views, using correspondences derived from epipolar-constrained visual features, thereby establishing multi-view consistency. SplatFlow [134] leverages a multi-view rectified flow (RF) model to simultaneously generate multi-view images, depth information, and camera poses based on text prompts. By incorporating training-free inversion and inpainting techniques, it achieves seamless editing of 3DGS. InterGSEdit [135] introduces a 3D Geometry-Consistent Attention Prior and an Adaptive Cross-Dimensional Attention Fusion Network to ensure multi-view consistency and enable fine-grained detail recovery.

- **Efforts towards Efficiency and Speed.** Additionally, to enhance the efficiency and speed of 3D editing, ProGDF [136] comprises Progressive Gaussian Sampling (PGS) and Gaussian Difference Field (GDF). PGS applies progressive constraints to generate diverse intermediate results during the editing process. GDF employs a lightweight neural network, leveraging these intermediate results to model the editing process, allowing for real-time, controllable, and flexible editing within a single training session. The optimization process of DreamCatalyst [36] approximates the reverse diffusion process, aligning with diffusion sampling dynamics and thereby reducing training time. 3DSceneEditor [137] utilizes a streamlined 3D pipeline, allowing direct manipulation of Gaussians. By leveraging input prompts, semantic labeling, and CLIP’s zero-shot capabilities, it enables efficient, high-quality editing. Chen *et al.* [133] propose Direct Gaussian Editor, which adapts 2D image editing models into a multi-view consistent version and integrates the 3D geometric representation of the underlying scene. This method enables direct optimization of the 3D representation, eliminating the need for iterative editing.

3DitScene [138] incorporates generative priors and optimization techniques to refine the 3D Gaussian model and utilizes language features extracted by CLIP for object disentanglement.

3.2.2 Editing Based on Image Prompt

Editing results that rely solely on text prompts often fail to fully meet user expectations, as textual descriptions may not sufficiently convey user preferences regarding details, styles, or specific appearances. To address this, some methods [139], [140], [141], [142] have begun incorporating image prompts as a supplement. Image prompts offer more intuitive and customized visual information, including color, texture, shape, and lighting details, enabling more precise visual guidance in the 3D editing process.

- **Parameter-Efficient Fine-Tuning.** To achieve personalized customization, it is necessary to learn from reference images and transfer them to the target object. TIP-Editor [33] introduces a progressive 2D personalization strategy that incorporates localized loss to ensure edits remain confined to user-defined regions. It employs LoRA [143] technology to fine-tune the text-to-image (T2I) model, binding the reference image to specific tokens for content personalization. Additionally, it utilizes explicit and flexible 3D Gaussian splatting as the 3D representation, enabling localized editing without altering the background. With a similar idea of [144], GS-VTON introduces a reference-driven image editing approach that integrates personalized information into a pre-trained 2D VTON model using LoRA fine-tuning. This method enables multi-view image editing while ensuring consistency across all views. In contrast, Cha et al. [145] propose PERSE, which learns a disentangled latent space from synthetic data to enable intuitive 3D facial editing, allowing attribute transfer from a reference image while preserving identity. Texture-GS [141] employs a UV mapping MLP, a local Taylor expansion of the MLP, and a learnable texture to decouple appearance from geometry by representing it as a 2D texture on a 3D surface.

- **Improving Multi-View Consistency with Diffusion Models.** Given their robust theoretical foundation and exceptional performance, diffusion models have naturally been widely adopted in the field of 3D editing. VcEdit [34] introduces the Cross-attention Consistency Module and the Editing Consistency Module, integrating 3DGS into the image editing process. This ensures that the edited guidance images maintain consistency across multiple views. Similarly, TIGER [146] introduces Coherent Score Distillation, which combines a 2D image editing diffusion model with a multi-view diffusion model to enhance score distillation, enabling multi-view consistent editing with finer details.

- **Multi-Stage Progressive Refinement.** The multi-stage approach, through phased processing, enables the model to preserve important details of the original image while enhancing the editing effects in the target regions, thereby better adapting to complex editing tasks. Point’n Move [147] additionally introduces 2D hint points as conditions and designs a two-stage self-prompting segmentation algorithm for mask refinement and merging, enabling real-time editing without requiring training for each edit. Jakub et al. [148] design a three-stage method: it begins with a set of input images and camera poses, utilizing a neural signed distance field (SDF) to reconstruct the scene surface, which guides the training of Gaussian splatting components to ensure alignment with the scene geometry. Finally, visual and geometric information is encoded into a lightweight triangle soup proxy. Edits are propagated through this intermediate structure to the mesh extracted from neural surface, thereby updating restored appearance.

GaussianVTON [149] pioneers a 3D Virtual Try-On pipeline by integrating Gaussian Splatting with 2D VTON, introducing a three-stage refinement strategy to enhance consistency.

3.2.3 Style Transfer

Unlike object manipulation tasks, style transfer requires preserving the structural integrity of the object while transferring the stylistic features from a reference image to the target image. This process typically involves the separation and recombination of low-level features (such as color and texture) and high-level features (such as semantic content) of the image.

- **Efforts towards Objective Function.** SGSST [150] designs a Simultaneously Optimized Scales loss, enabling style transfer across all scales for consistent multi-scale stylization. ReGS [151] improves stylization consistency via a Stylized Pseudo View Supervision loss for uniform appearance across views, and a Template Correspondence Matching loss to propagate style to occluded regions. WaSt-3D [152] performs style transfer directly on 3D Gaussians, using an entropy-regularized Wasserstein-2 distance to smoothly map the style scene distribution to the content scene via gradient flow, and decomposing stylization into smaller subproblems for efficiency. Multi-StyleGS [153] introduces a style loss with bipartite matching between multiple style image regions and GS points to enable local style transfer.

- **Efforts towards Integrating Diffusion Model.** InstantStyle-Gaussian [154] accelerates style editing by using a diffusion model to generate target style images, incorporating them into the training set, and iteratively optimizing the Gaussian splatting scene. ArtNVG [155] enhances control over content and style via the CSGO model and Tile ControlNet, and introduces an Attention-based Neighboring-View Alignment mechanism to maintain consistent colors and textures across neighboring views. Morpheus [156] employs an RGBD diffusion model with depth-guided cross-attention, feature injection, and a Warp ControlNet conditioned on composite frames to guide 3D stylization. FantasyStyle [157] proposes Controllable Stylized Distillation, achieving 3D style transfer solely through diffusion model distillation.

- **Efforts towards VGG Feature Optimization.** Saroha et al. [158] employ a pre-trained VGG model with AdaIN to transfer styles to specific views, training a 3D color module to predict new colors for each Gaussian. Similarly, StyleSplat [159] refines style transfer by applying a nearest neighbor feature matching loss between VGG features of the rendered image and the reference style image, and uses a 2D mask for selective stylization of specified objects. In contrast, StyleGaussian [160] embeds 2D VGG scene features into transformed 3D Gaussian features, combines them with reference image features, and decodes them into stylized RGB images. SemanticSplatStylization [161] integrates semantic understanding and uses VGG features to compute style loss, ensuring precise, context-aware stylization.

3.2.4 Other Editing Tasks

- **Object Removal.** Gaussian Grouping [22] uses 2D mask predictions from the SAM [48] to assign a compact identity encoding to each Gaussian, enabling direct manipulation of specified ones. In contrast, GScream [139] introduces multi-view monocular depth estimation as an additional constraint to optimize the placement of Gaussian primitives, improving the geometric alignment between the removed area and the surrounding region. Qiu et al. [162] propose the Feature Splatting method, which distills vision-language features into a 3D Gaussian representation to enable

semi-automatic scene decomposition via text queries, thereby facilitating scene editing operations such as object removal.

- **Drag.** MVDrag3D [163] employs a multi-view diffusion model as a robust generative prior to achieve consistent drag editing across multiple rendered views. DYG [164] uses 3D masks and control point pairs to define the target editing area and drag direction, leveraging the advantages of implicit tri-plane representation to establish a geometric framework for the editing results.

- **Video Editing.** 3DEgo [165] introduces a noise blending module to apply the diffusion model for video frame editing and leverages 3D Gaussian splatting to generate 3D scenes from multi-view consistent edited frames, reducing the multi-stage editing workflow to a single-stage process. PortraitGen [166] lifts 2D portrait video editing into 3D by integrating 3D human priors, ensuring both 3D and temporal consistency in the edited video.

- **Inpainting.** InFusion [167] uses an image-conditioned depth completion model to guide point initialization and directly recovers depth maps from images. ReFFusion [168] fine-tunes an image inpainting diffusion model, effectively aligning the prior distribution with the 3D target scene. This reduces score distillation variance and yields clearer details.

3.3 3DGS Generation

While NeRF-based methods produce high-quality 3D content, they are slow and computationally expensive. Recent advances in 3D Gaussian Splatting (3DGS) enable faster, more efficient 3D generation from text or images, categorized by the type of output.

3.3.1 Object-level Generation

A. Per-Scene Optimization Methods: Optimization-based methods extract diffusion priors from powerful 2D foundation diffusion models to guide and optimize 3D representations. DreamFusion [77] first introduces the Score Distillation Sampling (SDS) loss, which optimizes NeRF [2] using images generated from text prompts. Building on this, many methods [169], [170], [171], [172] have extensively explored optimization-based approaches.

- **Standard SDS-based Methods.** These methods directly use Score Distillation Sampling (SDS) to optimize 3D scenes. (a) *Text-to-3D.* Tanget *et al.* [9] extend 2D diffusion models to 3D by optimizing 3D Gaussians with SDS, introducing Mesh Extraction and Texture Refinement to mitigate SDS-induced blurriness. GS-GEN [173] and GaussianDreamer [40] incorporate 3D point cloud diffusion priors for geometry and appearance, while GaussianDreamerPro [174] adopts a geometry-guided framework to control Gaussian growth and enhance details. CompGS [175] decomposes scenes into entities for SDS optimization at entity and composition levels, dynamically adjusting spatial parameters for fine-grained details. CG3D [176] introduces a compositional framework for text-conditioned scene generation, producing detailed, multi-object, and plausible results. Hyper-3DG [177] refines Gaussians via a Geometry and Texture Hypergraph Refiner, and HCoG [178] hierarchically generates occlusion-aware assets. (b) *Image-to-3D.* ScalingGaussian [179] first generates point clouds with a 3D diffusion model, then refines Gaussians using a 2D diffusion model with SDS. Physics3D [180] simulates Gaussians via the Material Point Method (MPM) to estimate physical attributes and orientations, rendering them into video frames for SDS-based optimization with a pre-trained video diffusion model.

- **Efforts towards Improving SDS.** Although SDS provides guidance for 3D generation, it often suffers from low fidelity and

over-smoothing. Recent works address these issues by enhancing geometric accuracy, detail preservation, and stability. (a) *Text-to-3D.* StableDreamer [181] formulates the SDS prior and L2 reconstruction loss as equivalent, reducing multi-face artifacts and improving geometry. Li *et al.* [182] propose Guided Consistency Sampling integrated with 3DGS to enhance detail and fidelity. DreamMapping [183] introduces Variational Distribution Mapping, accelerating distribution modeling by treating rendered images as degraded diffusion outputs. HumanGaussian [184] designs a structure-aware SDS for joint optimization of human appearance and geometry. LucidDreamer [41] mitigates over-smoothing via Interval Score Matching (ISM) with deterministic diffusion trajectories, while TSM [185] extends ISM by generating two reverse DDIM [186] paths to reduce cumulative errors and pseudo-ground truth inconsistencies. GaussianMotion [187] employs adaptive score distillation to balance realism and smoothness. (b) *Image-to-3D.* Basak *et al.* [188] introduce a frequency-based distillation loss, extracting low-frequency geometry from 3D diffusion priors and refining high-frequency texture with 2D diffusion. GECO [189] adopts a two-stage pipeline combining Variational Score Distillation [190] and multi-view consistency refinement, enabling sub-second high-quality generation. DreamPhysics [191] leverages video diffusion priors to learn material properties and applies motion distillation sampling to emphasize dynamic cues.

- **Multi-View Guidance.** The imprecise guidance of SDS often leads to the Janus problem, characterized by multi-face ambiguity. MVGaussian [192], GradeADreamer [193], and GALA3D [194] mitigate this issue by combining SDS with MVDream [195] as a multi-view diffusion prior. GALA3D further incorporates layout-guided Gaussian representations and instance-level scene optimization to achieve high-fidelity object generation and realistic scene interactions. Li *et al.* [196] also adopt MVDream with hybrid Gaussian-mesh representations, introducing MVControl and SuGaR for controllable text-to-3D generation.

B. Feed-Forward-based Methods: Although these optimization-based methods have made significant progress in 3D content generation, they still face challenges such as lengthy optimization times. To address these issues, researchers have begun to shift towards feed-forward methods [197], [198], which involve training on large-scale datasets to directly generate 3D assets.

- **Latent-space Optimization.** These methods learn a latent space from conditional inputs such as RGB images, depth maps, or point clouds via an encoder, which is then decoded into 3D Gaussians. (a) *Text-to-3D.* Wizardwongsaet *et al.* [199] employ a feed-forward reconstruction encoder with pre-trained models to reduce training cost, refining unstructured latents via post-processing. They introduce a 2D perceptual rendering loss and a multi-stream transformer correction flow for efficient, high-quality text-conditioned generation. GaussianAnything [200] proposes a scalable framework with a point cloud-structured latent space, supporting multi-modal inputs, geometry-texture disentanglement, and 3D-aware editing. Atlas-Gaussians [201] use a patch-based encoder-decoder with UV sampling and a transformer decoder for efficient, high-fidelity Gaussian shape generation. Turbo3D [202] integrates a four-step, four-view latent diffusion generator with a feed-forward Gaussian reconstructor, employing a dual-teacher scheme for view consistency and photorealism while avoiding pixel-space decoding. (b) *Image-to-3D.* AGG [203] leverages a pre-trained DINOv2 [46] encoder and dual transformers to decode Gaussian position and texture fields for joint optimization. HumanSplat [204] encodes multi-view inputs via a VAE and applies

a latent reconstruction transformer interacting with structured human models. Zou *et al.* [205] design a hybrid triplane Gaussian latent representation from images and point clouds, decoded into 3D objects with transformer-based point and triplane decoders.

- **Multi-View-based Methods.** Incorporating multi-view inputs can substantially improve 3D generation quality. (a) *Text-to-3D*. Flex3D [206] adopts a two-stage framework: first, a fine-tuned multi-view image diffusion model and a video diffusion model generate a candidate view pool, filtered for quality and consistency via a view selection pipeline; second, selected views are processed by a transformer-based Flexible Reconstruction Model (FlexRM) that outputs 3D Gaussians using tri-plane representations for efficient, detailed generation. LGM [37] employs an asymmetric U-Net for high-resolution 3D Gaussian splatting, enabling expressive, scalable reconstruction from multi-view inputs without triplanes or transformers. (b) *Image-to-3D*. GS-LRM [39] uses a transformer architecture that patchifies posed images, processes concatenated multi-view tokens through transformer blocks, and decodes per-pixel Gaussian parameters for differentiable rendering. GEOGS3D [207] integrates orthogonal plane decomposition with a diffusion model to synthesize geometry-aware, multi-view consistent novel views, enhancing 3D object reconstruction.

- **Network Design.** Designing feed-forward networks tailored to 3DGS is an active research direction. (a) *Text-to-3D*. BrightDreamer [208] proposes a fast feed-forward framework combining a text-guided shape deformation network with a triplane generator to efficiently predict and optimize Gaussian attributes. (b) *Image-to-3D*. Lu *et al.* [209] present the Point-to-Gaussian Generator composed of multiple APP blocks, each with a point feature extractor, projection module, and cross-modal attention, followed by multi-linear heads to decode 3D Gaussians. GRM [38] introduces an upsampler using a windowed self-attention variant to capture non-local cues and enhance high-frequency details. UniGS [210] develops a DETR-like framework treating Gaussians as queries, updated via multi-view cross-attention over input images to mitigate ghosting artifacts.

- **Optimization Diffusion Models.** These methods directly produce 3D Gaussians by fine-tuning or training diffusion models. (a) *Text-to-3D*. GVGEN [198] adopts a structured Gaussian volume representation and a coarse-to-fine pipeline, using a candidate pool strategy for pruning and densification to reconstruct high-fidelity 3D scenes from complex text. (b) *Image-to-3D*. NovelGS [211] generates 3D Gaussians from sparse-view images with novel-view denoising, achieving state-of-the-art reconstruction with consistent, sharp textures. Ouroboros3D [212] jointly trains multi-view image generation and 3D reconstruction in a recursive diffusion process, enabling mutual adaptation for robust inference. Cycle3D [213] cyclically integrates 2D diffusion-based generation and feed-forward 3D reconstruction to improve multi-view consistency and texture quality. DiffusionGS [214] outputs Gaussian point clouds at each timestep for view-consistent generation from any direction, introducing a scene-object mixed training strategy to enhance scalability. Hi3D [215] employs a video diffusion paradigm with 3D-aware priors and video-to-video refinement for consistent multi-view reconstruction.

3.3.2 Scene-level Generation

A. Per-Scene Optimization Methods: These methods optimize each scene individually to generate high-quality 3D Gaussians. (a) *Text-to-3D*. DreamScene [43] builds on CSD [216], a variant of SDS, by integrating information across multiple timesteps during

sampling, obtaining rich semantic guidance from 2D diffusion models. FastScene [217] proposes a Progressive Novel View Inpainting for generating refined views. DreamScene360 [44] uses text-based panorama priors for 3D scene generation with 3DGS to maintain multi-view consistency, and mitigates invisibility in single-view inputs via semantic and geometric regularization. (b) *Image-to-3D*. Zhong *et al.* [218] introduce scene-grounding guidance in video diffusion models to improve sequence consistency and handle extrapolation and occlusion. WonderWorld [219] proposes Fast Layered Gaussian Surfels (FLAGS) for scene generation, incorporating guided depth diffusion to reduce geometric distortion. Scene4U [220] combines LLMs and segmentation models to decompose panoramic images into layers, enabling multi-layered 3D scene generation.

B. Iterative Generation Methods: These approaches iteratively refine 3D Gaussian representations through repeated rendering and optimization to achieve high-quality scene reconstruction. (a) *Text-to-3D*. Text2Room [42] combines monocular depth estimation with a text-conditioned inpainting model, aligning scene frames with existing geometry for 3D reconstruction. Text2Immersion [221] progressively generates Gaussian point clouds using 2D diffusion and depth models, followed by refinement via interpolation. RealmDreamer [222] initializes points with a text-to-image generator, lifts them into 3D, computes occlusion volumes, and optimizes across multiple views using an image-conditioned diffusion model. WonderJourney [223] employs LLMs to generate scene descriptions, builds 3D scenes via text-driven point cloud generation, and validates them with VLMs. HoloDreamer [224] addresses global inconsistency and incompleteness by generating high-resolution panoramas for holistic initialization, followed by rapid 3DGS-based reconstruction for view-consistent, enclosed scenes. (b) *Image-to-3D*. LucidDreamer [225] alternates between Dreaming, which generates multi-view consistent images guided by a point cloud, and Alignment, which integrates new 3D points into a unified scene, producing realistic 3D Gaussian splats from text, RGB, or RGBD inputs. VistaDream [226] enforces multi-view consistency during reverse diffusion sampling to improve temporal coherence. Kang *et al.* [227] propose a transformer-based latent diffusion model with explicit view geometry constraints, incorporating warped feature maps, epipolar-weighted source features, Plücker ray maps, and camera poses for high-quality novel view generation.

C. Feed-Forward-based Methods: Similar to object-level generation, feed-forward approaches have also been explored.

- **Network Design.** (a) *Text-to-3D*. TextSplat [228] introduces Text-Guided Semantic Fusion Module to integrate multi-source semantic features under sentence-level guidance, enhancing geometry semantic consistency. (b) *Image-to-3D*. PixelSplat [229] employs a multi-view epipolar transformer to address scale ambiguity, while MVSplat [4] and Splatter360 [230] construct planar or spherical cost volumes for improved geometry estimation. MVSplat360 [231] leverages pre-trained video diffusion for 3D-consistent views. GaussianCity [232] adopts BEV-Point as a compact intermediate representation with a spatial-aware decoder. SelfSplat [233] introduces matching-aware pose estimation and depth refinement to ensure geometric consistency. CATSplat [234] fuses vision-language text features with point cloud features via transformer blocks, and OmniSplat [235] uses a Yin-Yang grid to reduce distortion.

- **Optimization Diffusion Models.** (a) *Text-to-3D*. Prometheus [236] sequentially trains GS-VAE and MV-LDM for direct text-to-

3D scene generation. VideoRFSplat [237] couples a pose generation model with a pretrained video generator via communication blocks to produce multi-view images and camera poses. (b) *Image-to-3D*. ViewCrafter [238] employs a point-conditioned video diffusion model for high-quality 3D scenes, while Wonderland [239] integrates diverse camera trajectories via a dual-branch conditioning mechanism for view-consistent latents. GGS [240] combines 3D representations with latent video diffusion and a custom decoder to synthesize scenes from feature fields. VideoScene [241] distills video diffusion through a 3D-aware leap flow strategy for one-step generation. SceneSplatter [242] adopts a momentum-based paradigm to balance generative priors and existing scene information during generation.

3.4 Other Application Tasks

3.4.1 Human Avatar

Human avatars, digital representations of users in virtual spaces, enable immersive interaction across gaming, virtual meetings, and the metaverse. 3DGS-based avatar modeling can be divided into two main directions: 1) Body-based avatars [243], [244], [245], [246], [247], [248] typically rely on parametric body models like SMPL [249] or SMPL-X [250] to guide canonical Gaussian initialization. Methods such as HUGS [247] and Animatable Gaussians [243] extend beyond rigid skeletons by introducing pose-conditioned deformation to handle garments and fine motions. Others like D3GA [251] and GauHuman [252] enhance realism with cage-based deformation or efficient monocular reconstruction to move beyond rigid templates. Despite progress, body-based methods still face challenges in handling loose clothing, fast motions, and generalization to unseen scenes. 2) Head-based avatars [6], [253], [254], [255] emphasize fine-grained reconstruction of facial geometry, expressions, and speech-driven dynamics. Many approaches combine FLAME [256] with deformable Gaussians to capture subtle expressions. For instance, Gaussian Head Avatar [257] replaces traditional LBS with MLP-based displacement, while FlashAvatar [111] achieves 300 FPS real-time rendering. Despite progress, Head-based methods still face challenges in handling subtle facial expressions, uneven illumination, and low-quality pose.

3.4.2 SLAM

Simultaneous Localization and Mapping (SLAM) is a foundational task in robotics and vision, aiming to estimate camera poses and reconstruct 3D environments simultaneously. We broadly categorize 3DGS-based SLAM [258], [259], [260], [261] into two directions: geometry-based SLAM and semantics-aware SLAM. The former includes RGB-D SLAM and RGB SLAM, depending on depth availability. RGB-D SLAM methods (e.g., GS-SLAM [5], SplatAM [262]) leverage accurate depth to construct dense Gaussian maps and enable reliable tracking via silhouette rendering or Gaussian matching. In contrast, RGB SLAM (e.g., MonoGS [263], Photo-SLAM [264]) must infer geometry through multi-view optimization or depth prediction, posing challenges in outdoor or dynamic scenes due to less stable depth cues. Beyond geometry, semantic SLAM incorporates scene understanding to enable richer 3D maps for downstream tasks like navigation and interaction. Early works like SGS-SLAM [265] embed semantic colors into Gaussians, while more recent methods (e.g., OpenGS-SLAM [266], GS³LAM [267], LEGS [268]) introduce learned

semantic features or language-guided Gaussians to enhance high-level reasoning. Such semantic integration improves robustness, particularly under sensor noise or ambiguous geometry. Despite progress, open challenges remain, like SLAM under sparse views, scalable memory, and consistent semantics in large-scale scenes.

3.4.3 3DGS Object Detection

3D object detection focuses on identifying and localizing objects in 3D space. Similar to segmentation, detection methods can be categorized into prompt-based and generic approaches. Prompt-based detection, often referred to as open-vocabulary detection or visual grounding, takes textual inputs (e.g., category names or language expressions) and outputs object locations. Most 3DGS-based segmentation methods also support this type of detection by generating the maximum response point, and are thus not detailed here. Specifically, SpatialReasoner [269] combines LLM-driven spatial reasoning with a hierarchical feature field enhanced by visual properties. It distills CLIP and SAM features and leverages fine-tuned LLMs to infer spatial instructions, enabling precise localization of target instances based on relational language cues. For generic object detection, representative methods include: Gaussian-Det [270], which models objects continuously using input Gaussians as feature descriptors across partial surfaces; 3DGS-DET [271], which incorporates boundary guidance and box-focused sampling to refine Gaussian distributions and suppress background noise; and MATT-GS [272], which employs masked attention 3D Gaussian Splatting to enhance object localization.

4 PERFORMANCE COMPARISON

This section compares different methods across tasks. For each task, we introduce the datasets and evaluation metrics, followed by detailed result tables. Fig. 3 shows examples from 13 commonly used datasets in segmentation, editing, and generation.

4.1 Performance Benchmarking: 3DGS Segmentation

• **Datasets.** Table 1 summarizes the key features of the datasets for 3DGS segmentation, followed by detailed descriptions.

ScanNet [274] contains 1,513 RGB-D sequences from 707 indoor scenes, offering 2.5M frames with 3D reconstructions, camera poses, and dense semantic/instance annotations. It includes 36K labeled objects across 20 categories and is a standard benchmark for indoor scene understanding.

Replica [279] is a high-quality indoor 3D dataset with dense geometry, HDR textures, accurate material properties (e.g., glass, mirrors), planar segmentation, and semantic/instance annotations, supporting realistic simulation and scene understanding.

NVOS [273] is a segmentation-focused extension of LLFF with undistorted images, mask and scribble annotations, designed for language-guided 2D-to-3D segmentation.

Mip-NeRF [275] provides unbounded real-world scenes with precise poses for 360° novel view synthesis.

SPIn-NeRF [66] contains 10 real-world forward-facing scenes with annotated object masks. Each scene includes 60 training images with the object and 40 test images without the object.

3D-OVS [61] is a benchmark for open-vocabulary 3D segmentation with language-aligned semantic labels, containing 10 scenes with around 30 360° images each.

LERF-OVS [26] contains open-vocabulary semantic annotations for 4 scenes derived from the LERF dataset [60].

TABLE 1: Statistics of representative 3DGS segmentation datasets. See §4.1 for more detailed descriptions.

Dataset	Venue	#Scene	#Views(Avg.)	Characterization
ScanNet [274]	[CVPR'17]	1513	1500	Large-scale RGB-D scans with 3D poses and semantics for advanced scene understanding.
Replica [279]	[ArXiv'19]	18	175	High-quality indoor scans with geometry, HDR textures, and rich semantic labels.
NVOS [273]	[CVPR'21]	8	36	Built on LLFF with undistorted images, annotated with masks and scribbles for segmentation tasks.
Mip-NeRF 360 [275]	[CVPR'22]	9	215	Focusing on capturing complex lighting, geometry, and texture details.
SPIn-NeRF [66]	[CVPR'23]	10	100	Providing challenging real-world scenes with views both with and without a target object.
3D-OVS [61]	[NeurIPS'23]	10	30	Including high-quality 3D objects spanning diverse categories with language-aligned semantic labels.
LERF-OVS [26]	[CVPR'24]	4	200	An extended version of LERF dataset with ground truth mask annotations for open-vocabulary segmentation.
LERF-Mask [22]	[ECCV'24]	3	200	Containing semantic annotations of three scenes from LERF dataset [60] with a total of 23 prompts.
Ref-LERF [7]	[ICML'25]	4	200	Focusing on spatial relationships, annotated with natural language expressions for referring 3DGS segmentation.
SceneSplat-7K [121]	[ICCV'25]	7k	-	The first large-scale, high-quality 3DGS dataset for indoor environments boosting scene understanding research.
SceneSplat-49K [280]	[ArXiv'25]	49k	-	Containing diverse indoor and outdoor scenes, featuring complex, high-quality full scenes from multiple sources.



Fig. 3: Examples from 13 commonly used datasets for segmentation, editing, and generation.

LERF-Mask [22] contains semantic annotations of three scenes from LERF dataset [60] with a total of 23 prompts.

Ref-LERF [7] extends the LERF dataset [60] with 295 language expressions referring to 59 objects in 4 scenes, emphasizing spatial relationships to support referring segmentation [282], [283] in 3DGS.

SceneSplat-7K [121] is the first large-scale, high-quality 3DGS dataset for indoor environments, containing 7,916 scenes aggregated from seven well-established datasets.

SceneSplat-49K [280] is a curated dataset of diverse indoor and outdoor scenes, featuring complex, high-quality full-scene 3DGS

TABLE 2: Quantitative 3D instance segmentation on Replica [279], and LERF-Mask [22]. Following [20], we report mIoU and F-score on Replica, and mIoU and mBIoU on LERF-Mask.

Method	Venue	Type	Replica [279]		LERF-Mask [22]	
			mIoU(%)	F-score(%)	mIoU(%)	mBIoU(%)
GaussianGrouping [22]	[ECCV'24]	Pre-Process.	23.6	30.4	72.8	67.6
OmniSeg3D [18]	[CVPR'24]	Post-Process.	39.1	35.9	74.7	71.8
Gaga [19]	[ArXiv'24]	Pre-Process.	-	-	74.7	72.2
Unified-Lift [20]	[CVPR'25]	End-to-End	41.6	43.9	80.9	77.1

TABLE 3: Quantitative 3D interactive segmentation on NVOS [281], SPIn-NeRF [66] in terms of mIoU and mAcc.

Method	Venue	Train	Input	NVOS [281]		SPIn-NeRF [66]	
				mIoU(%)	mAcc(%)	mIoU(%)	mAcc(%)
SA3D-GS [102]	[NeurIPS'23]	✓	2D Click/Text	90.7	98.3	93.2	99.1
SAGD [23]	[ArXiv'24]	✗	2D Click/Text	90.4	98.2	89.9	98.7
FlashSplat [111]	[ECCV'24]	✗	2D Click	91.8	98.6	-	-
Click-Gaussian [24]	[ECCV'24]	✓	2D Click	-	-	94.0	-
GaussianCut [29]	[NeurIPS'24]	✗	2D Click/Text	92.5	98.4	92.9	99.2
SAGA [30]	[AAAI'25]	✓	2D Click/Text	90.9	98.3	88.0	98.5
COB-GS [109]	[CVPR'25]	✓	Text	92.1	98.6	-	-
iSegMan [25]	[CVPR'25]	✗	2D Click	92.0	98.4	92.4	99.1
LUDVIG [114]	[ICCV'25]	✗	Text	92.4	-	93.8	-

TABLE 4: Performance comparison of open-vocabulary 3D semantic segmentation on ScanNet [274] benchmark. The evaluation metrics are mIoU and mAcc, respectively.

Method	Venue	Evaluation	19 classes		15 classes		10 classes	
			mIoU	mAcc	mIoU	mAcc	mIoU	mAcc
LangSplat [26]	[CVPR'24]	Point	3.8	9.1	5.4	13.2	8.4	22.1
LEGaussians [83]	[CVPR'24]	Point	3.8	10.9	9.0	22.2	12.8	28.6
OpenGaussian [32]	[NeurIPS'24]	Point	24.7	41.5	30.1	48.3	38.3	55.2
InstanceGaussian [31]	[CVPR'25]	Point	40.7	54.0	42.5	59.2	47.9	64.0
PanoGS [110]	[CVPR'25]	Point	50.7	70.2	-	-	-	-
Dr. Splat [117]	[CVPR'25]	Gaussian	28.0	44.6	38.2	60.4	47.2	68.9
CAGS [101]	[ArXiv'25]	Gaussian	32.6	48.9	41.1	62.0	54.8	75.9

reconstructions from multiple sources.

• **Metrics.** Common evaluation metrics in the segmentation domain are outlined below:

Mean Intersection over Union (mIoU) measures segmentation accuracy by computing the average IoU across all classes, where IoU is the ratio between the intersection and the union of predicted and ground truth regions for each class.

Mean Accuracy (mAcc) measures the proportion of correctly predicted pixels or instances over the total, reflecting the overall correctness of the segmentation or classification results.

Mean Boundary Intersection over Union (mBIoU) computes the average IoU over narrow boundary regions, emphasizing boundary precision compared to standard mIoU.

Panoptic Quality (PQ) calculates panoptic segmentation performance by recognition quality (RQ) and segmentation quality (SQ). **F-score** measures the balance between precision and recall, computed using an IoU threshold of 0.5.

• **Results.** Following the taxonomy in Sec.2.1.1, we report results across four representative segmentation settings. For 3D instance segmentation (Table 2), Unified-Lift [20] achieves the best overall performance on both the Replica [279] and LERF-Mask [22] datasets, demonstrating the effectiveness of consistency-aware end-to-end learning. In the setting of 3D interactive segmentation (Table 3), GaussianCut [29] performs best on NVOS [273], while Click-Gaussian [24] attains the highest mIoU on SPIn-NeRF [66].

TABLE 5: Quantitative open-vocabulary 2D semantic segmentation on 3D-OVS [61] dataset in terms of mIoU.

Method	Venue	Foundation Model	Bed	Bench	Room	Sofa	Lawn	Mean
LangSplat [26]	[CVPR'24]	CLIP & SAM	92.5	94.2	94.1	90.0	96.1	93.4
Feature3DGS [27]	[CVPR'24]	CLIP	83.5	90.7	84.7	86.9	93.4	87.8
LEGaussians [83]	[CVPR'24]	CLIP	84.9	91.1	86.0	87.8	92.5	88.5
GaussianGrouping [22]	[ECCV'24]	SAM	83.0	91.5	85.9	87.3	90.6	87.7
N2F2 [86]	[ECCV'24]	CLIP & SAM	93.8	92.6	93.5	92.1	96.3	93.9
GOI [94]	[MM'24]	APE [284] & CLIP	89.4	92.8	91.3	85.6	94.1	90.6
FMGS [93]	[ICCV'24]	CLIP & DINO	80.6	84.5	87.9	90.8	92.6	87.3
SLGaussian [115]	[ArXiv'24]	CLIP & SAM	41.3	47.0	-	30.3	54.4	44.1
FMLGS [96]	[ArXiv'25]	SAM2 & CLIP	95.7	96.3	96.8	95.2	-	96.0
SAGA [30]	[AAAI'25]	CLIP & SAM	97.4	95.4	96.8	93.5	96.6	96.0
FastLGS [95]	[AAAI'25]	CLIP & SAM	94.7	95.1	95.3	90.6	96.2	94.4
econSG [105]	[ICLR'25]	SAM	94.9	93.0	95.8	91.6	96.3	94.3
VLGaussian [28]	[ICLR'25]	CLIP	96.8	97.3	97.7	95.5	97.9	97.1
LBG [113]	[WACV'25]	CLIP & SAM & DINO	97.7	96.3	95.9	97.3	87.4	94.9
CLIP-GS [92]	[TOMM'25]	SAM	97.2	94.8	-	94.1	96.5	95.6
CCL-LGS [106]	[ICCV'25]	SAM & CLIP	97.3	95.0	-	92.3	96.1	95.2
ObjectGS [285]	[ICCV'25]	SAM2	98.0	96.4	95.1	97.2	95.4	96.4

TABLE 6: Quantitative Results on LERF-OVS [26] Dataset.

We report the open-vocabulary localization accuracy (mAcc) and 2D semantic segmentation (mIoU).

Method	Venue	Ramen mIoU mAcc	Figurines mIoU mAcc	Teamtime mIoU mAcc	Kitchen mIoU mAcc
LangSplat [26]	[CVPR'24]	51.2 73.2	44.7 80.4	65.1 88.1	44.5 95.5
Feature3DGS [27]	[CVPR'24]	43.7 69.8	40.5 73.4	58.8 77.2	39.6 87.6
LEGaussians [83]	[CVPR'24]	46.0 67.5	40.8 75.2	60.3 75.6	39.4 90.3
GaussianGrouping [22]	[ECCV'24]	45.5 68.6	40.0 74.3	60.9 75.0	38.7 88.2
N2F2 [86]	[ECCV'24]	56.6 78.8	47.0 85.7	69.2 91.5	47.9 95.5
FMGS [93]	[ICCV'24]	- 90.0	- 93.8	- 89.7	- 92.6
GOI [94]	[MM'24]	52.6 75.5	44.5 82.9	63.7 88.6	41.4 90.4
LangSurf [87]	[ArXiv'24]	47.0 63.4	- -	73.6 84.8	55.0 81.9
FMLGS [96]	[ArXiv'25]	73.2 89.2	72.4 94.3	81.8 96.7	64.3 96.2
FastLGS [95]	[AAAI'25]	- 84.2	- 91.4	- 95.0	- 96.2
econSG [105]	[ICLR'25]	- 83.2	- 89.3	- 93.4	- 96.2
VLGaussian [28]	[ICLR'25]	61.4 92.5	58.1 97.1	73.5 95.8	54.8 98.6
LangScene-X [119]	[ICCV'25]	42.9 72.7	- -	45.0 78.9	63.6 90.9
LUDVIG [114]	[ICCV'25]	58.1 78.9	63.3 80.4	77.1 94.9	58.5 90.9
CCL-LGS [106]	[ICCV'25]	62.3 -	61.2 -	71.8 -	67.1 -

Notably, GaussianCut is a training-free method that flexibly supports both 2D clicks and text prompts as input. For open-vocabulary 3D semantic segmentation (Table 4), PanoGS [110] and InstanceGaussian [31] achieve the best performance under point-based evaluation protocols, whereas CAGS [101] performs best under 3D Gaussian-based evaluation. In the open-vocabulary 2D semantic segmentation setting, VLGaussian [28] reaches a state-of-the-art mIoU of 97.1% on the 3D-OVS benchmark [61], significantly outperforming existing approaches in Table 5. Table 6 further presents results for two subtasks: open-vocabulary 2D localization (detection) and semantic segmentation. FMLGS [96] achieves the best performance on the segmentation task, while VLGaussian [28] leads in localization. Across these settings, most methods leverage powerful vision-language foundation models such as CLIP and SAM to enhance open-vocabulary capabilities.

4.2 Performance Benchmarking: 3DGS Editing

• **Datasets.** We summarize the key features of the datasets in Table 7, with detailed descriptions provided below.

DTU [286] containing 80 scenes of large variability. Each scene consists of 49 or 64 accurate camera positions and reference structured light scans, all acquired by a 6-axis industrial robot.

Tanks and Temples [287] consists of 21 scenes, including individual objects such as “Tank” and “Train,” as well as large indoor scenes like “Auditorium” and “Museum”.

GL3D [288] contains 125,623 high-resolution images, mostly drone-captured at varying scales and angles with strong geometric overlap, covering urban, rural, and scenic areas.

LLFF [289] consists of both synthetic and real-world datasets. The synthetic part includes rendered images from 45,000 simplified indoor scenes, while the real-world part covers 24 training scenes and 8 testing scenes, each with 20–30 multi-view images.

NeRF-synthetic [2] consists of 8 scenes of an object placed on a white background. Each scene includes 100 training images with a resolution of 800×800 and associated camera poses.

BlendedMVS [290] contains 113 scenes with 20–1000 images each, totaling 17,818 images.

Co3D [291] contains 1.5 million frames from 19,000 videos of objects across 50 MS-COCO categories, with camera poses and 3D point cloud annotations.

Mip-NeRF360 [275] provides 360° indoor and outdoor panoramas for evaluating neural rendering methods, focusing on complex lighting, geometry, and textures.

Nerfstudio [292] contains 10 scenes: 4 captured by phones with pinhole lenses and 6 by mirrorless cameras with fisheye lenses.

SPIn-NeRF [66] contains 10 forward-facing in-the-wild scenes, including 3 indoor and 7 outdoor scenes, each with 100 multi-view images and annotated foreground masks.

IN2N [74] contains 6 real-world scenes (*e.g.*, bear, face, person), each with an average of 172 images.

ScanNet++ [293] contains 460 scenes, 280,000 captured DSLR images, and over 3.7M iPhone RGBD frames.

360-USID [294] includes 4 outdoor and 3 indoor scenes, each with 171–347 training and 31–33 novel views.

• **Metrics.** Commonly used evaluation metrics in the editing domain are listed below:

CLIP Text-Image Direction Similarity. CLIP [47] extracts two paired sets of text-image embeddings (original and modified), and computes their directional shifts via cosine similarity.

CLIP Text-Image Similarity. CLIP [47] measures text-image similarity by encoding text and images into embeddings separately and then computing their cosine similarity.

CLIP Image-Image Similarity. CLIP [47] computes image-image similarity by encoding edited image and subject image into embeddings separately and then computing their cosine similarity.

Frechet Inception Distance (FID) calculates the similarity between ground truth and generated images by comparing their Inception-v3 [295] feature distributions using the Frechet distance.

DINO Similarity. DINO [296] extracts features from the edited scene and reference image, then computes their average visual similarity to evaluate image-image alignment.

Peak Signal-to-Noise Ratio (PSNR) measures image quality by comparing the maximum pixel intensity to the MSE between images, converted to decibels.

Structural Similarity (SSIM) measures image similarity by comparing brightness, contrast, and structure.

RMSE. It is computed as the root mean squared pixel-wise difference between the edited image and ground truth.

Learned Perceptual Image Patch Similarity (LPIPS) measures perceptual similarity by comparing deep features of two images.

Aesthetic score. Aesthetic Predictor V2.5 [297] is a SigLIP-based model that rates image aesthetics from 1 to 10.

User study. It evaluates results by collecting and analyzing feedback from human participants across customized dimensions such as preference in comparative results, text-image alignment, and view consistency.

• **Results.** For 3D image editing tasks, the most commonly used datasets are Mip-NeRF360 [275] and IN2N [74]. We adopt these two datasets as benchmarks to record the performance of various methods. However, as most existing 3D editing methods are evaluated on different scene subsets, it remains difficult to perform a comprehensive and fair comparison under a unified protocol. Given that IN2N [74] is widely adopted as a baseline, we report

TABLE 7: Statistics of representative 3DGS editing datasets. See §4.2 for more detailed descriptions.

Dataset	Venue	#Scenes	#Views(Avg.)	Characterization
DTU [286]	[CVPR'14]	80	343	Each scene consists of 49 or 64 accurate camera positions and reference structured light scans.
Tanks and Temples [287]	[TOG'17]	14	-	It includes individual objects (e.g., 'Tank', 'Train') and large indoor scenes (e.g., 'Auditorium', 'Museum').
GL3D [288]	[ACCV'18]	543	230	It contains 125,623 high-resolution images, most of which were captured by drones from multiple scales and perspectives with significant geometric overlap. The images cover urban areas, rural regions, and scenic spots.
LLFF [289]	[TOG'19]	32	25	Using the COLMAP structure from motion implementation to compute poses for our real images.
NeRF-synthetic [2]	[ECCV'20]	8	100	Each object is placed on a white background, with images at 800x800 resolution and corresponding camera poses.
BlendedMVS [290]	[CVPR'20]	113	158	A large-scale MVS dataset, which contains a total of 17,818 images.
Co3D [291]	[CVPR'21]	-	-	Consists of 1.5 million frames extracted from approximately 19,000 videos, capturing objects from 50 MS-COCO categories. Each image is annotated with camera poses and ground-truth 3D point clouds.
Mip-NeRF360 [275]	[CVPR'22]	9	215	It consists of 360-degree panoramic images from both indoor and outdoor scenes.
Nerfstudio [292]	[SIGGRAPH'23]	10	-	4 phone captures with pinhole lenses and 6 mirrorless camera captures with a fisheye lens.
SPin-NeRF [66]	[CVPR'23]	10	100	Providing challenging real-world scenes with views both with and without a target object.
IN2N [74]	[ICCV'23]	6	172	Enabling structured and globally consistent 3D scene modifications while preserving the original scene's identity.
ScanNet++ [293]	[ICCV'23]	460	608	280,000 captured DSLR images, and over 3.7M iPhone RGBD frames.
360-USID [294]	[CVPR'25]	7	300	Four outdoor (Box, Cone, Lawn, Plant) and three indoor (Cookie, Sunflower, Dustpan).

TABLE 8: Performance comparison of 3DGS editing on Mip-NeRF360 [275] and IN2N [74] datasets. The similarity for CLIP Text-Image Direction, CLIP Text-Image, CLIP Image-Image, DINO are denoted as $CLIP_{dir}$, $CLIP_{T2I}$, $CLIP_{I2I}$, and $DINO_{sim}$, respectively.

Methods	Venue	Category	Condition	2D Model	$CLIP_{dir}$ ↑	$CLIP_{T2I}$ ↑	$CLIP_{I2I}$ ↑	$DINO_{sim}$ ↑	FID ↓	PSNR ↑	SSIM ↑	FPS ↓
IN2N [74]	[ICCV'23]				Baseline							
GaussianEditor [8]	[CVPR'24]	Localizing the Editing Object	Text	InstructPix2Pix [122]	+29.44%	-	-	-	-	-	-	-
GaussianEditor [35]	[CVPR'24]	Localizing the Editing Object	Text	InstructPix2Pix [122]	+27.27%	-	+11.76%	-	-50.49%	-	-	-60.87%
TIP-Editor [33]	[TOG'24]	Parameter-Efficient Tuning	Text&Image	Stable Diffusion [55]	+86.75%	-	-	+8.52%	-	-	-	-
GaussCtrl [130]	[ECCV'24]	Multi-View Consistency	Text	ControlNet [196]	+19.34%	-	-	-	-	-	-	-33.33%
DGE [133]	[ECCV'24]	Multi-View Consistency	Text	InstructPix2Pix [122]	+4.69%	+5.12%	-	-	-	-	-	-92.16%
GaussianVTON [149]	[ArXiv'24]	Multi-Stage Refinement	Image	Stable Diffusion [55]	-	+105.81%	+23.29%	-	-40.47%	+28.39%	+11.61%	-
Eyal et al. [132]	[ArXiv'24]	Multi-View Consistency	Text	Stable Diffusion [55]	+26.00%	+9.09%	+10.50%	+43.44%	-	+2.37%	-	-
ProGDF [136]	[ArXiv'24]	Efficiency and Speed	Text	InstructPix2Pix [122]	+36.25%	-	-	-	-	-	-	-
TrAME [131]	[TMM'25]	Multi-View Consistency	Text	Stable Diffusion [55]	-	-	+9.15%	-	-	+16.60%	-	-
DreamCatalyst [36]	[ICLR'25]	Efficiency and Speed	Text	InstructPix2Pix [122]	+10.14%	-	+1.04%	-	-	-	-	-46.15%

TABLE 9: Performance comparison of 3DGS style transfer on Mip-NeRF360 [275] dataset, evaluated by LPIPS and RMSE.

Method	Venue	2D Model	Short-Term Consis. LPIPS ↓	Short-Term Consis. RMSE ↓	Long-Term Consis. LPIPS ↓	Long-Term Consis. RMSE ↓
StyleGaus. [160]	[SIGGRAPH'24]	VGG	0.033	0.029	0.055	0.063
SemanticSplatSty. [161]	[TEGA'24]	VGG	0.019	0.042	0.028	0.055
InstantStyleGaus. [154]	[ArXiv'24]	Diffusion	0.024	0.026	0.074	0.076
SGSST [150]	[CVPR'25]	VGG	0.030	0.032	0.055	0.063

the relative gains of each method over IN2N to enable an indirect yet relatively fair comparison, as summarized in Table 8. Overall, GaussianVTON [149] demonstrates the best performance across multiple metrics. For the style transfer task, we use Mip-NeRF 360 [275] as the benchmark and compare the results of different methods in Table 9, where SemanticSplatSty. [161] achieves the best overall performance.

4.3 Performance Benchmarking: 3DGS Generation

• **Datasets.** We summarize the key features of the datasets in Table 10, with detailed descriptions provided below.

NYUdepth [298] contains 1449 RGBD images, capturing 464 diverse indoor scenes, with detailed annotations.

ShapeNet [278] contains approximately 50,000 3D models across 55 object categories. Each model includes a corresponding geometry file and a unique identifier.

ScanNet [274] is a large RGB-D dataset containing 2.5 M views in 1,513 indoor scenes annotated with 3D camera poses.

RealEstate10K [299] contains 67,477 training and 7,289 testing home walkthrough video scenes from YouTube.

Replica [279] is a dataset of 18 highly photorealistic 3D indoor scenes, each with dense meshes, HDR textures, semantic and instance labels, and reflective surfaces like mirrors and glass.

ACID [300] featuring aerial landscape videos, includes 11,075 training scenes and 1,972 testing scenes.

GSO [277] comprises 1,030 3D scanned household items.

LAION-5B [301] consists of three subsets: 2.32 billion English image-text pairs, 2.26 billion image-text pairs in over 100 other languages, and 1.27 billion samples with undetectable language.

Objaverse [276] is a large-scale dataset of objects with 800K+ (and growing) 3D models with descriptive captions, tags, and animations.

OmniObject3D [302] contains 6,000 scanned objects across 190 daily categories. Each object includes textured meshes, point clouds, multiview renders, and real-captured videos.

LOM [303] comprises five real-world scenes ("buu", "chair", "sofa", "bike", and "shrub"), each containing 25 to 48 sRGB images captured by a DJI Osmo Action 3 camera under adverse lighting conditions, including low light and overexposure.

G-objaverse [304]. Derived from Objaverse [276], G-Objaverse filters out poorly captioned 3D models and includes high-quality renderings produced via a hybrid of rasterization and path tracing.

• **Metrics.** Common evaluation metrics we used are listed below:

MLLM evaluation use multimodal large language models (e.g., GPT-4, LLaVA [311]) to evaluate generation quality from multiple dimensions. Common evaluation metrics include BLIP-VQA [312], CLIP-IQA [313], Q-Align [314] and others.

Natural Image Quality Evaluator (NIQE) computes image quality by extracting natural scene statistics from image patches, comparing them to a Gaussian model trained on pristine images, and calculating the deviation as a quality score.

Blind/Referenceless Image Spatial Quality Evaluator (BRISQUE) estimates perceptual quality by extracting natural scene statistics from locally normalized luminance and applying a regression model trained on human-rated distorted images.

Kernel Inception Distance measures distributional differences between real and generated images by computing maximum mean discrepancy with polynomial kernels on Inception-v3 features.

Chamfer distance computes the similarity between two point sets by computing the average closest-point distance in both directions.

Thresholded Symmetric Epipolar Distance (TSED) calculates the number of consistent frame pairs in a sequence.

Inception Score evaluate the quality of generated images using Inception-V3 [295].

CMMD [315] is based on richer CLIP embeddings and the maximum mean discrepancy with the Gaussian RBF kernel.

TABLE 10: Statistics of representative 3DGS generation datasets. See §4.3 for more detailed descriptions.

Dataset	Venue	#Type	#Scenes	Characterization
NYUdepth [298]	[ECCV'12]	Image-to-3D	464	It contains 1449 RGBD images, capturing 464 diverse indoor scenes, with detailed annotations.
ShapeNet [278]	[ArXiv'15]	Image&Text-to-3D	60k	These 3D models span 55 categories, each with a geometry file and unique identifier.
ScanNet [274]	[CVPR'17]	Image-to-3D	1513	It contains 2.5 M views in 1513 indoor scenes annotated with 3D camera poses.
RealEstate10K [299]	[SIGGRAPH'18]	Image-to-3D	80k	It comprises home walkthrough videos from YouTube.
Replica [279]	[ArXiv'19]	Image-to-3D	18	A 3D indoor scene dataset featuring dense meshes, HDR textures, and semantic labels.
ACID [300]	[ICCV'21]	Image-to-3D	13047	Featuring aerial landscape videos, includes 11,075 training scenes and 1,972 testing scenes.
GSO [277]	[ICRA'22]	Image&Text-to-3D	1030	It comprises 3D scanned common household items.
LAION-5B [301]	[NeurIPS'22]	Text-to-3D	-	LAION-5B's key feature is its vast scale, with 5.85 billion image-text pairs.
Objaverse [276]	[CVPR'23]	Image&Text-to-3D	800K	Objaverse has vast scale of 800K+ 3D models with rich annotations.
OmniObject3D [302]	[CVPR'23]	Image-to-3D	6k	A large-scale collection of high-quality real-scanned 3D objects with rich 2D and 3D annotations.
LOM [303]	[AAAI'24]	Image-to-3D	5	Includes five real-world scenes, each with 25–48 sRGB images captured in difficult lighting.
G-objaverse [304]	[ECCV'24]	Image&Text-to-3D	280K	10 general classes which gives about 280K samples

TABLE 11: Quantitative 3DGS generation on GSO [277] dataset. CLIP Image-Image Similarity as CLIP_{I2I}.

Methods	Venue	Category	Condition	2D Foundation Model	PSNR↑	SSIM↑	LPIPS↓	CLIP _{I2I} ↑	FID↓	KID↓
Per-Scene Optimization										
DreamGaussian [9]	[ICLR'24]	Standard SDS	Text&Image	Stable Diffusion [55]	18.27	0.834	0.189	0.748	-	-
Hritam et al. [188]	[ArXiv'24]	Standard SDS	Image	Stable Diffusion [55]	22.16	0.887	0.121	-	-	-
GECO [189]	[ArXiv'24]	Improving SDS	Image	Zero123++ [305]	19.31	0.825	0.154	-	-	-
Feed-Forward-based										
LGM [37]	[ECCV'24]	Multi-View-based	Text&Image	MVDream [195]	17.13	0.810	0.250	-	19.93	0.55
GRM [38]	[ECCV'24]	Network Design	Text&Image	Zero123++ [305]	25.03	0.899	0.102	0.869	-	-
GS-LRM [39]	[ECCV'24]	Multi-View-based	Image	Zero123++ [305]	17.70	0.795	0.241	-	112.96	-
Lu et al. [209]	[MM'24]	Network Design	Image	-	17.92	0.810	0.210	-	-	-
Hi3D [215]	[MM'24]	Optimization Diffusion	Image	Stable Video Diffusion [306]	24.26	0.864	0.119	-	-	-
DiffusionGS [214]	[ArXiv'24]	Optimization Diffusion	Image	FLUX & SD [55]	22.07	0.854	0.111	-	11.52	-
GeoGS3D [207]	[ArXiv'24]	Multi-View-based	Image	Zero-1-to-3 [307]	22.98	0.899	0.146	-	-	-
NovelGS [211]	[ArXiv'24]	Optimization Diffusion	Text&Image	-	31.30	0.946	0.065	-	-	-
Cycle3D [213]	[AAAI'25]	Optimization Diffusion	Image	MVDream [195]	21.40	0.884	0.115	0.855	-	-
GaussianAnything [200]	[ICLR'25]	Latent Optimization	Text&Image	-	-	-	-	-	24.21	0.76
Flex3D [206]	[ICML'25]	Multi-View-based	Image	Emu Model [308]	25.55	0.894	0.074	0.893	-	-
Ouroboros3D [212]	[CVPR'25]	Optimization Diffusion	Image	Stable Video Diffusion [306]	21.76	0.889	0.109	-	-	-

TABLE 12: Quantitative 3DGS generation on Objaverse [276] dataset. CLIP Text-Image Similarity as CLIP_{T2I}.

Methods	Venue	Category	Condition	2D Foundation Model	PSNR↑	SSIM↑	LPIPS↓	CLIP _{T2I} ↑	FID↓	KID↓
Feed-Forward-based										
LGM [37]	[ECCV'24]	Multi-View-based	Text&Image	MVDream [195]	-	-	-	27.21	123.8	4.53
GVGEN [198]	[ECCV'24]	Optimization Diffusion	Text	Stable Diffusion [55]	-	-	-	27.33	132.4	6.04
GeoGS3D [207]	[ArXiv'24]	Multi-View-based	Image	Zero-1-to-3 [307]	23.97	0.921	0.113	-	-	-
Wizadwongsa et al. [199]	[ArXiv'24]	Latent Optimization	Text	Stable Diffusion 3 [309]	-	-	-	27.61	-	-
Atlas-Gaussians [201]	[ICLR'25]	Latent Optimization	Text	Latent Diffusion Model [55]	-	-	-	30.66	109.5	4.04
Turbo3D [202]	[CVPR'25]	Latent Optimization	Text	DiT [310]	-	-	-	27.61	-	-

HPSv2 [316] is a scoring model that more accurately predicts human preferences for generated images.

User study. It evaluates results by gathering human feedback on preferences, appearance quality, and geometric quality.

- **Results.** We select two representative datasets, GSO [277] and Objaverse [276], as benchmarks for 3DGS generation. The performance of various methods is summarized in Table 11 and Table 12, respectively. Due to the limited number of publicly comparable baselines, we provide a quantitative assessment based on the available results. On GSO dataset, NovelGS [211] achieves the best performance by tailoring the diffusion process to suit the 3D Gaussian representation. It supports both text-to-3D and image-to-3D generation, demonstrating strong generalization across input modalities. On Objaverse dataset, Atlas-Gaussians [201] performs best, leveraging latent space optimization to enhance generation quality. It primarily supports text-conditioned generation and shows promising results on open-domain content.

5 FUTURE DIRECTIONS

- **Large-Scale Feed-Forward Learning.** To overcome the inefficiency of per-scene optimization, especially under dense calibrated images conditions, more and more methods adopt feed-forward architectures to enable fast and generalizable segmentation, editing, and generation. In the future, future research should explore large-scale training regimes across diverse scenarios and domains. This includes scaling up data volume, improving data diversity (e.g., egocentric, indoor, outdoor), and designing robust pipelines that generalize beyond static, clean environments.

- **Faithful Evaluation Metrics.** Current evaluation protocols often inherit metrics from traditional 2D or NeRF-based tasks, which

may not align well with 3DGS goals. Developing reliable and interpretable metrics specifically designed for evaluating application tasks from a 3D Gaussian perspective is essential to track progress and guide future research. Existing metrics primarily focus on 2D projection image-level accuracy, lacking meaningful insights into the inherent 3D geometric and semantic consistency of generated or edited scenes. Establishing 3D-aware metrics is promising.

- **Integrating Large Language Models.** Combining 3DGS with Large Language Models (LLMs) opens new opportunities for semantic understanding and instruction-based manipulation, such as text-driven editing, generation, and open-vocabulary understanding. Research is needed to build effective 3D-text alignment and prompting strategies. Leveraging LLMs to reason over spatial relationships and affordances in 3D scenes also presents promising avenues for embodied intelligence and interactive applications.

- **Synthesizing 3D Data.** Given the persistent shortage of annotated 3D data, future research can leverage the generative capabilities of 3DGS to synthesize large-scale, high-quality 3D datasets from abundant 2D image collections. Such synthetic datasets could significantly enhance training data diversity and volume, ultimately driving substantial improvements in the performance of 3DGS application tasks. Additionally, combining synthesized data with domain adaptation techniques could further bridge the domain gap between synthetic and real-world data, enhancing the model's robustness and generalization capabilities.

- **Toward Generalist Models.** Instead of designing separate models for segmentation, editing, and generation, a promising direction is to develop generalist 3DGS-based architectures that can perform multiple scene-level tasks within a unified framework. Developing such versatile models can facilitate the sharing of learned representations across tasks, resulting in improved efficiency, reduced

redundancy in training, and enhanced generalization capabilities.

• **Combining 3D Foundation Model.** Emerging 3D foundation models such as VGGT [317] and FLARE [318] provide robust representations by pretraining on diverse 3D tasks, including depth estimation, correspondence, and pose prediction from multi-view images. These models encode rich geometric priors that can benefit various downstream applications. Future work may incorporate them into 3DGS to improve generalization and efficiency.

6 CONCLUSION

This survey systematically explores recent advances in utilizing 3D Gaussian Splatting (3DGS) for downstream application tasks, representing a pioneering effort in summarizing this emerging field. We first introduce essential background knowledge, covering fundamental concepts and foundational models. Subsequently, we comprehensively review over 150 representative methods across several key tasks, including segmentation, editing, generation, and other related application tasks, providing a structured categorization from a technical perspective. Furthermore, we present a thorough analysis of existing benchmarks and conduct fair comparisons of representative models clearly. Lastly, we highlight current challenges and outline promising future directions to inspire continued research efforts toward enhanced high-level tasks.

REFERENCES

- [1] B. Kerbl, G. Kopanas, T. Leimkühler, and G. Drettakis, “3d gaussian splatting for real-time radiance field rendering,” *ACM TOG*, 2023.
- [2] B. Mildenhall, P. P. Srinivasan, M. Tancik, J. T. Barron, R. Ramamoorthi, and R. Ng, “Nerf: Representing scenes as neural radiance fields for view synthesis,” in *ECCV*, 2020.
- [3] T. Lu, M. Yu, L. Xu, Y. Xiangli, L. Wang, D. Lin, and B. Dai, “Scaffoldgs: Structured 3d gaussians for view-adaptive rendering,” in *CVPR*, 2024.
- [4] Y. Chen, H. Xu, C. Zheng, B. Zhuang, M. Pollefeys, A. Geiger, T.-J. Cham, and J. Cai, “Mvsplat: Efficient 3d gaussian splatting from sparse multi-view images,” in *ECCV*, 2024.
- [5] C. Yan, D. Qu, D. Xu, B. Zhao, Z. Wang, D. Wang, and X. Li, “Gs-slam: Dense visual slam with 3d gaussian splatting,” in *CVPR*, 2024.
- [6] S. Qian, T. Kirschstein, L. Schoneveld, D. Davoli, S. Giebenhain, and M. Nießner, “Gaussianavatars: Photorealistic head avatars with rigged 3d gaussians,” in *CVPR*, 2024.
- [7] S. He, G. Jie, C. Wang, Y. Zhou, S. Hu, G. Li, and H. Ding, “ReferSplat: Referring segmentation in 3d gaussian splatting,” in *ICML*, 2025.
- [8] Y. Chen, Z. Chen, C. Zhang, F. Wang, X. Yang, Y. Wang, Z. Cai, L. Yang, H. Liu, and G. Lin, “Gaussianeditor: Swift and controllable 3d editing with gaussian splatting,” in *CVPR*, 2024.
- [9] J. Tang, J. Ren, H. Zhou, Z. Liu, and G. Zeng, “Dreamgaussian: Generative gaussian splatting for efficient 3d content creation,” in *ICLR*, 2024.
- [10] G. Chen and W. Wang, “A survey on 3d gaussian splatting,” *arXiv preprint arXiv:2401.03890*, 2024.
- [11] S. Zhu, G. Wang, X. Kong, D. Kong, and H. Wang, “3d gaussian splatting in robotics: A survey,” *arXiv preprint arXiv:2410.12262*, 2024.
- [12] M. T. Bagdasarian, P. Knoll, Y.-H. Li, F. Barthel, A. Hilsmann, P. Eisert, and W. Morgenstern, “3dgs. zip: A survey on 3d gaussian splatting compression methods,” *arXiv preprint arXiv:2407.09510*, 2024.
- [13] M. S. Ali, C. Zhang, M. Cagnazzo, G. Valenzise, E. Tartaglione, and S.-H. Bae, “Compression in 3d gaussian splatting: A survey of methods, trends, and future directions,” *arXiv preprint arXiv:2502.19457*, 2025.
- [14] T. Wu, Y.-J. Yuan, L.-X. Zhang, J. Yang, Y.-P. Cao, L.-Q. Yan, and L. Gao, “Recent advances in 3d gaussian splatting,” *Computational Visual Media*, 2024.
- [15] B. Fei, J. Xu, R. Zhang, Q. Zhou, W. Yang, and Y. He, “3d gaussian splatting as new era: A survey,” *IEEE TVCG*, 2024.
- [16] Y. Bao, T. Ding, J. Huo, Y. Liu, Y. Li, W. Li, Y. Gao, and J. Luo, “3d gaussian splatting: Survey, technologies, challenges, and opportunities,” *IEEE TCSVT*, 2025.
- [17] M.-B. Jurca, R. Royen, I. Giosan, and A. Munteanu, “Rt-gs2: Real-time generalizable semantic segmentation for 3d gaussian representations of radiance fields,” *BMVC*, 2024.
- [18] H. Ying, Y. Yin, J. Zhang, F. Wang, T. Yu, R. Huang, and L. Fang, “Omniseg3d: Omniversal 3d segmentation via hierarchical contrastive learning,” in *CVPR*, 2024.
- [19] W. Lyu, X. Li, A. Kundu, Y.-H. Tsai, and M.-H. Yang, “Gaga: Group any gaussians via 3d-aware memory bank,” *arXiv preprint arXiv:2404.07977*, 2024.
- [20] R. Zhu, S. Qiu, Z. Liu, K.-H. Hui, Q. Wu, P.-A. Heng, and C.-W. Fu, “Rethinking end-to-end 2d to 3d scene segmentation in gaussian splatting,” in *CVPR*, 2025.
- [21] W. Hu, W. Chai, S. Hao, X. Cui, X. Wen, J.-N. Hwang, and G. Wang, “Pointmap association and piecewise-plane constraint for consistent and compact 3d gaussian segmentation field,” *arXiv*, 2025.
- [22] M. Ye, M. Danelljan, F. Yu, and L. Ke, “Gaussian grouping: Segment and edit anything in 3d scenes,” in *ECCV*, 2024.
- [23] X. Hu, Y. Wang, L. Fan, J. Fan, J. Peng, Z. Lei, Q. Li, and Z. Zhang, “Sagd: Boundary-enhanced segment anything in 3d gaussian via gaussian decomposition,” *arXiv preprint arXiv:2401.17857*, 2024.
- [24] S. Choi, H. Song, J. Kim, T. Kim, and H. Do, “Click-gaussian: Interactive segmentation to any 3d gaussians,” in *ECCV*, 2024.
- [25] Y. Zhao, W. Xu, R. Zheng, P. Qiao, C. Liu, and J. Chen, “isegman: Interactive segment-and-manipulate 3d gaussians,” in *CVPR*, 2025.
- [26] M. Qin, W. Li, J. Zhou, H. Wang, and H. Pfister, “Langsplat: 3d language gaussian splatting,” in *CVPR*, 2024.
- [27] S. Zhou, H. Chang, S. Jiang, Z. Fan, Z. Zhu, D. Xu, P. Chari, S. You, Z. Wang, and A. Kadambi, “Feature 3dgs: Supercharging 3d gaussian splatting to enable distilled feature fields,” in *CVPR*, 2024.
- [28] Q. Peng, B. Planche, Z. Gao, M. Zheng, A. Choudhuri, T. Chen, C. Chen, and Z. Wu, “3d vision-language gaussian splatting,” *ICLR*, 2025.
- [29] U. Jain, A. Mirzaei, and I. Gilitschenski, “Gaussiancut: Interactive segmentation via graph cut for 3d gaussian splatting,” in *NeurIPS*, 2024.
- [30] J. Cen, J. Fang, C. Yang, L. Xie, X. Zhang, W. Shen, and Q. Tian, “Segment any 3d gaussians,” in *AAAI*, 2025.
- [31] H. Li, Y. Wu, J. Meng, Q. Gao, Z. Zhang, R. Wang, and J. Zhang, “Instancegaussian: Appearance-semantic joint gaussian representation for 3d instance-level perception,” *CVPR*, 2024.
- [32] Y. Wu, J. Meng, H. Li, C. Wu, Y. Shi, X. Cheng, C. Zhao, H. Feng, E. Ding, J. Wang *et al.*, “Opengaussian: Towards point-level 3d gaussian-based open vocabulary understanding,” in *NeurIPS*, 2024.
- [33] J. Zhuang, D. Kang, Y.-P. Cao, G. Li, L. Lin, and Y. Shan, “Tip-editor: An accurate 3d editor following both text-prompts and image-prompts,” *ACM TOG*, 2024.
- [34] Y. Wang, X. Yi, Z. Wu, N. Zhao, L. Chen, and H. Zhang, “View-consistent 3d editing with gaussian splatting,” in *ECCV*, 2024.
- [35] J. Wang, J. Fang, X. Zhang, L. Xie, and Q. Tian, “Gaussianeditor: Editing 3d gaussians delicately with text instructions,” in *CVPR*, 2024.
- [36] J. Kim, S. Lee, J. Shin, J. Choi, and H. Shim, “Dreamcatalyst: Fast and high-quality 3d editing via controlling editability and identity preservation,” in *ICLR*, 2025.
- [37] J. Tang, Z. Chen, X. Chen, T. Wang, G. Zeng, and Z. Liu, “Lgm: Large multi-view gaussian model for high-resolution 3d content creation,” in *ECCV*, 2024.
- [38] Y. Xu, Z. Shi, W. Yifan, H. Chen, C. Yang, S. Peng, Y. Shen, and G. Wetzstein, “Grm: Large gaussian reconstruction model for efficient 3d reconstruction and generation,” in *ECCV*, 2024.
- [39] K. Zhang, S. Bi, H. Tan, Y. Xiangli, N. Zhao, K. Sunkavalli, and Z. Xu, “Gs-lrm: Large reconstruction model for 3d gaussian splatting,” in *ECCV*, 2024.
- [40] T. Yi, J. Fang, J. Wang, G. Wu, L. Xie, X. Zhang, W. Liu, Q. Tian, and X. Wang, “Gaussiandreamer: Fast generation from text to 3d gaussians by bridging 2d and 3d diffusion models,” in *CVPR*, 2024.
- [41] Y. Liang, X. Yang, J. Lin, H. Li, X. Xu, and Y. Chen, “Luciddreamer: Towards high-fidelity text-to-3d generation via interval score matching,” in *CVPR*, 2024.
- [42] L. Höllein, A. Cao, A. Owens, J. Johnson, and M. Nießner, “Text2room: Extracting textured 3d meshes from 2d text-to-image models,” in *ICCV*, 2023.
- [43] H. Li, H. Shi, W. Zhang, W. Wu, Y. Liao, L. Wang, L.-h. Lee, and P. Y. Zhou, “Dreamscene: 3d gaussian-based text-to-3d scene generation via formation pattern sampling,” in *ECCV*, 2024.
- [44] S. Zhou, Z. Fan, D. Xu, H. Chang, P. Chari, T. Bharadwaj, S. You, Z. Wang, and A. Kadambi, “Dreamscene360: Unconstrained text-to-3d scene generation with panoramic gaussian splatting,” in *ECCV*, 2024.

- [45] M. Caron, H. Touvron, I. Misra, H. Jégou, J. Mairal, P. Bojanowski, and A. Joulin, “Emerging properties in self-supervised vision transformers,” in *ICCV*, 2021.
- [46] M. Oquab, T. Darcet, T. Moutakanni, H. Vo, M. Szafraniec, V. Khalidov, P. Fernandez, D. Haziza, F. Massa, A. El-Nouby *et al.*, “Dinov2: Learning robust visual features without supervision,” *TMLR*, 2024.
- [47] A. Radford, J. W. Kim, C. Hallacy, A. Ramesh, G. Goh, S. Agarwal, G. Sastry, A. Askell, P. Mishkin, J. Clark *et al.*, “Learning transferable visual models from natural language supervision,” in *ICML*, 2021.
- [48] A. Kirillov, E. Mintun, N. Ravi, H. Mao, C. Rolland, L. Gustafson, T. Xiao, S. Whitehead, A. C. Berg, W.-Y. Lo *et al.*, “Segment anything,” in *ICCV*, 2023.
- [49] N. Ravi, V. Gabeur, Y.-T. Hu, R. Hu, C. Ryali, T. Ma, H. Khedr, R. Rädle, C. Rolland, L. Gustafson *et al.*, “Sam 2: Segment anything in images and videos,” in *ICLR*, 2025.
- [50] H. Ding, K. Ying, C. Liu, S. He, X. Jiang, Y.-G. Jiang, P. H. Torr, and S. Bai, “MOSEv2: A more challenging dataset for video object segmentation in complex scenes,” *arXiv preprint arXiv:2508.05630*, 2025.
- [51] H. Ding, C. Liu, S. He, X. Jiang, P. H. Torr, and S. Bai, “MOSE: A new dataset for video object segmentation in complex scenes,” in *ICCV*, 2023.
- [52] H. Ding, C. Liu, S. He, X. Jiang, and C. C. Loy, “MeViS: A large-scale benchmark for video segmentation with motion expressions,” in *ICCV*, 2023.
- [53] H. Ding, C. Liu, S. He, K. Ying, X. Jiang, C. C. Loy, and Y.-G. Jiang, “MeViS: A multi-modal dataset for referring motion expression video segmentation,” *IEEE TPAMI*, 2025.
- [54] J. Ho, A. Jain, and P. Abbeel, “Denoising diffusion probabilistic models,” *NeurIPS*, 2020.
- [55] R. Rombach, A. Blattmann, D. Lorenz, P. Esser, and B. Ommer, “High-resolution image synthesis with latent diffusion models,” in *CVPR*, 2022.
- [56] S. Zhi, T. Laidlow, S. Leutenegger, and A. J. Davison, “In-place scene labelling and understanding with implicit scene representation,” in *CVPR*, 2021.
- [57] S. Kobayashi, E. Matsumoto, and V. Sitzmann, “Decomposing nerf for editing via feature field distillation,” *NeurIPS*, 2022.
- [58] V. Tschernezki, I. Laina, D. Larlus, and A. Vedaldi, “Neural feature fusion fields: 3d distillation of self-supervised 2d image representations,” in *3DV*, 2022.
- [59] R. Goel, D. Sirikonda, S. Saini, and P. Narayanan, “Interactive segmentation of radiance fields,” in *CVPR*, 2023.
- [60] J. Kerr, C. M. Kim, K. Goldberg, A. Kanazawa, and M. Tancik, “Lerf: Language embedded radiance fields,” in *ICCV*, 2023.
- [61] K. Liu, F. Zhan, J. Zhang, M. Xu, Y. Yu, A. El Saddik, C. Theobalt, E. Xing, and S. Lu, “Weakly supervised 3d open-vocabulary segmentation,” *NeurIPS*, 2023.
- [62] B. Wang, L. Chen, and B. Yang, “Dm-nerf: 3d scene geometry decomposition and manipulation from 2d images,” in *ICLR*, 2023.
- [63] Q. Wu, X. Liu, Y. Chen, K. Li, C. Zheng, J. Cai, and J. Zheng, “Object-compositional neural implicit surfaces,” in *ECCV*, 2022.
- [64] Y. Siddiqui, L. Porzi, S. R. Buló, N. Müller, M. Nießner, A. Dai, and P. Kotschieder, “Panoptic lifting for 3d scene understanding with neural fields,” in *CVPR*, 2023.
- [65] Y. Bhalgat, I. Laina, F. Henriques, A. Zisserman, and A. Vedaldi, “Contrastive lift: 3d object instance segmentation by slow-fast contrastive fusion,” in *NeurIPS*, 2023.
- [66] A. Mirzaei, T. Aumentado-Armstrong, K. G. Derpanis, J. Kelly, M. A. Brubaker, I. Gilitschenski, and A. Levinstein, “Spin-nerf: Multiview segmentation and perceptual inpainting with neural radiance fields,” in *CVPR*, 2023.
- [67] J. Cen, Z. Zhou, J. Fang, W. Shen, L. Xie, D. Jiang, X. Zhang, Q. Tian *et al.*, “Segment anything in 3d with nerfs,” in *NeurIPS*, 2023.
- [68] C. M. Kim, M. Wu, J. Kerr, K. Goldberg, M. Tancik, and A. Kanazawa, “Garfield: Group anything with radiance fields,” in *CVPR*, 2024.
- [69] S. Liu, X. Zhang, Z. Zhang, R. Zhang, J.-Y. Zhu, and B. Russell, “Editing conditional radiance fields,” in *CVPR*, 2021.
- [70] C. Wang, M. Chai, M. He, D. Chen, and J. Liao, “Clip-nerf: Text-and-image driven manipulation of neural radiance fields,” in *CVPR*, 2022.
- [71] B. Yang, Y. Zhang, Y. Xu, Y. Li, H. Zhou, H. Bao, G. Zhang, and Z. Cui, “Learning object-compositional neural radiance field for editable scene rendering,” in *ICCV*, 2021.
- [72] A. Mirzaei, Y. Kant, J. Kelly, and I. Gilitschenski, “Laterf: Label and text driven object radiance fields,” in *ECCV*, 2022.
- [73] K. Kania, K. M. Yi, M. Kowalski, T. Trzcinski, and A. Tagliasacchi, “Conerf: Controllable neural radiance fields,” in *CVPR*, 2022.
- [74] A. Haque, M. Tancik, A. A. Efros, A. Holynski, and A. Kanazawa, “Instruct-nerf2nerf: Editing 3d scenes with instructions,” in *ICCV*, 2023.
- [75] K. Schwarz, Y. Liao, M. Niemeyer, and A. Geiger, “Graf: Generative radiance fields for 3d-aware image synthesis,” *NeurIPS*, 2020.
- [76] Y. Deng, J. Yang, J. Xiang, and X. Tong, “Gram: Generative radiance manifolds for 3d-aware image generation,” in *CVPR*, 2022.
- [77] B. Poole, A. Jain, J. T. Barron, and B. Mildenhall, “Dreamfusion: Text-to-3d using 2d diffusion,” *ICLR*, 2023.
- [78] C.-H. Lin, J. Gao, L. Tang, T. Takikawa, X. Zeng, X. Huang, K. Kreis, S. Fidler, M.-Y. Liu, and T.-Y. Lin, “Magic3d: High-resolution text-to-3d content creation,” in *CVPR*, 2023.
- [79] G. Metzger, E. Richardson, O. Patashnik, R. Giryes, and D. Cohen-Or, “Latent-nerf for shape-guided generation of 3d shapes and textures,” in *CVPR*, 2023.
- [80] H. Wang, X. Du, J. Li, R. A. Yeh, and G. Shakhnarovich, “Score jacobian chaining: Lifting pretrained 2d diffusion models for 3d generation,” in *CVPR*, 2023.
- [81] E. R. Chan, C. Z. Lin, M. A. Chan, K. Nagano, B. Pan, S. De Mello, O. Gallo, L. J. Guibas, J. Tremblay, S. Khamis *et al.*, “Efficient geometry-aware 3d generative adversarial networks,” in *CVPR*, 2022.
- [82] J. Zhang, X. Li, Z. Wan, C. Wang, and J. Liao, “Text2nerf: Text-driven 3d scene generation with neural radiance fields,” *IEEE TVCG*, 2024.
- [83] J.-C. Shi, M. Wang, H.-B. Duan, and S.-H. Guan, “Language embedded 3d gaussians for open-vocabulary scene understanding,” in *CVPR*, 2024.
- [84] Z. Gao, L. Li, L. Jiao, F. Liu, X. Liu, W. Ma, Y. Guo, and S. Yang, “Fast and efficient: Mask neural fields for 3d scene segmentation,” *arXiv preprint arXiv:2407.01220*, 2024.
- [85] B. Li, K. Q. Weinberger, S. Belongie, V. Koltun, and R. Ranftl, “Language-driven semantic segmentation,” in *ICLR*, 2022.
- [86] Y. Bhalgat, I. Laina, J. F. Henriques, A. Zisserman, and A. Vedaldi, “N2f2: Hierarchical scene understanding with nested neural feature fields,” in *ECCV*, 2024.
- [87] H. Li, R. Qin, Z. Zou, D. He, B. Li, B. Dai, D. Zhang, and J. Han, “Langsurf: Language-embedded surface gaussians for 3d scene understanding,” *arXiv preprint arXiv:2412.17635*, 2024.
- [88] H. Yin, H. Zhan, Y. Xu, and R. A. Yeh, “Semantic consistent language gaussian splatting for point-level open-vocabulary querying,” *arXiv preprint arXiv:2503.21767*, 2025.
- [89] S. Liang, S. Wang, K. Li, M. Niemeyer, S. Gasperini, N. Navab, and F. Tombari, “Supergseg: Open-vocabulary 3d segmentation with structured super-gaussians,” *arXiv preprint arXiv:2412.10231*, 2024.
- [90] J. Guo, X. Ma, Y. Fan, H. Liu, and Q. Li, “Semantic gaussians: Open-vocabulary scene understanding with 3d gaussian splatting,” *arXiv preprint arXiv:2403.15624*, 2024.
- [91] J. Qiu, L. Liu, Z. Su, and T. Lin, “Gls: Geometry-aware 3d language gaussian splatting,” *arXiv preprint arXiv:2411.18066*, 2024.
- [92] G. Liao, J. Li, Z. Bao, X. Ye, J. Wang, Q. Li, and K. Liu, “Clip-gs: Clip-informed gaussian splatting for real-time and view-consistent 3d semantic understanding,” *ACM TOMM*, 2025.
- [93] X. Zuo, P. Samangouei, Y. Zhou, Y. Di, and M. Li, “Fmgs: Foundation model embedded 3d gaussian splatting for holistic 3d scene understanding,” *IJCV*, 2024.
- [94] Y. Qu, S. Dai, X. Li, J. Lin, L. Cao, S. Zhang, and R. Ji, “Goi: Find 3d gaussians of interest with an optimizable open-vocabulary semantic-space hyperplane,” in *ACM MM*, 2024.
- [95] Y. Ji, H. Zhu, J. Tang, W. Liu, Z. Zhang, X. Tan, and Y. Xie, “Fastlgs: Speeding up language embedded gaussians with feature grid mapping,” in *AAAI*, 2025.
- [96] X. Tan, Y. Ji, H. Zhu, and Y. Xie, “Fmlgs: Fast multilevel language embedded gaussians for part-level interactive agents,” *arXiv*, 2025.
- [97] Z. Dai, T. Liu, and Y. Zhang, “Efficient decoupled feature 3d gaussian splatting via hierarchical compression,” in *CVPR*, 2025.
- [98] Z. Li, W. Han, Y. Cai, H. Jiang, B. Bi, S. Gao, H. Zhao, and Z. Wang, “Gradiseg: Gradient-guided gaussian segmentation with enhanced 3d boundary precision,” *arXiv preprint arXiv:2412.00392*, 2024.
- [99] B. Dou, T. Zhang, Y. Ma, Z. Wang, and Z. Yuan, “Cosseggaussians: Compact and swift scene segmenting 3d gaussians,” *arXiv*, 2024.
- [100] Y. Lu, Y. Zhou, Y. Qiao, C. Song, T. Liang, J. Ma, and Y. Yin, “Segment then splat: A unified approach for 3d open-vocabulary segmentation based on gaussian splatting,” *arXiv preprint arXiv:2503.22204*, 2025.
- [101] W. Sun, Y. Zhou, J. Jiao, and Y. Li, “Cags: Open-vocabulary 3d scene understanding with context-aware gaussian splatting,” *arXiv*, 2025.
- [102] J. Cen, J. Fang, Z. Zhou, C. Yang, L. Xie, X. Zhang, W. Shen, and Q. Tian, “Segment anything in 3d with radiance fields,” *IJCV*, 2025.
- [103] M. C. Silva, M. Dahaghin, M. Toso, and A. Del Bue, “Contrastive gaussian clustering: Weakly supervised 3d scene segmentation,” *ICPR*, 2024.

- [104] J. Piekenbrinck, C. Schmidt, A. Hermans, N. Vaskevicius, T. Linder, and B. Leibe, "Opensplat3d: Open-vocabulary 3d instance segmentation using gaussian splatting," in *CVPRW*, 2025.
- [105] C. Zhang and G. H. Lee, "econsg: Efficient and multi-view consistent open-vocabulary 3d semantic gaussians," in *ICLR*, 2025.
- [106] L. Tian, X. Li, L. Ma, H. Huang, Z. Zheng, H. Yin, T. Li, H. Lu, and X. Jia, "Ccl-lgs: Contrastive codebook learning for 3d language gaussian splatting," in *ICCV*, 2025.
- [107] M. Jiang, S. Jia, J. Gu, X. Lu, G. Zhu, A. Dong, and L. Zhang, "Vote-splat: Hough voting gaussian splatting for 3d scene understanding," in *ICCV*, 2025.
- [108] S. Jang and W. Kim, "Identity-aware language gaussian splatting for open-vocabulary 3d semantic segmentation," in *ICCV*, 2025.
- [109] J. Zhang, J. Jiang, Y. Chen, K. Jiang, and X. Liu, "Cob-gs: Clear object boundaries in 3dgs segmentation based on boundary-adaptive gaussian splitting," in *CVPR*, 2025.
- [110] H. Zhai, H. Li, Z. Li, X. Pan, Y. He, and G. Zhang, "Panogs: Gaussian-based panoptic segmentation for 3d open vocabulary scene understanding," in *CVPR*, 2025.
- [111] Q. Shen, X. Yang, and X. Wang, "Flashsplat: 2d to 3d gaussian splatting segmentation solved optimally," in *ECCV*, 2024.
- [112] S. Dai, Y. Qu, Z. Li, X. Li, S. Zhang, and L. Cao, "Training-free hierarchical scene understanding for gaussian splatting with superpoint graphs," *arXiv preprint arXiv:2504.13153*, 2025.
- [113] R. Chacko, N. Haeni, E. Khaliullin, L. Sun, and D. Lee, "Lifting by gaussians: A simple, fast and flexible method for 3d instance segmentation," in *WACV*, 2025.
- [114] J. Marrie, R. Ménégaux, M. Arbel, D. Larlus, and J. Mairal, "Ludvig: Learning-free uplifting of 2d visual features to gaussian splatting scenes," in *ICCV*, 2025.
- [115] K. Chen, B. Dai, M. Qin, D. Zhang, P. Li, Y. Zou, and H. Wang, "Sigaussian: Fast language gaussian splatting in sparse views," *arXiv preprint arXiv:2412.08331*, 2024.
- [116] X. Wang, C. Lan, H. Zhu, Z. Chen, and Y. Lu, "Gsemsplat: Generalizable semantic 3d gaussian splatting from uncalibrated image pairs," *arXiv preprint arXiv:2412.16932*, 2024.
- [117] K. Jun-Seong, G. Kim, K. Yu-Ji, Y.-C. F. Wang, J. Choe, and T.-H. Oh, "Dr. splat: Directly referring 3d gaussian splatting via direct language embedding registration," in *CVPR*, 2025.
- [118] Q. Li, J. Sun, L. An, Z. Su, H. Zhang, and Y. Liu, "Semanticsplat: Feed-forward 3d scene understanding with language-aware gaussian fields," *arXiv preprint arXiv:2506.09565*, 2025.
- [119] F. Liu, H. Li, J. Chi, H. Wang, M. Yang, F. Wang, and Y. Duan, "Langscene-x: Reconstruct generalizable 3d language-embedded scenes with trimap video diffusion," in *ICCV*, 2025.
- [120] Z. Yang, J. Teng, W. Zheng, M. Ding, S. Huang, J. Xu, Y. Yang, W. Hong, X. Zhang, G. Feng *et al.*, "Cogvideox: Text-to-video diffusion models with an expert transformer," in *ICLR*, 2025.
- [121] Y. Li, Q. Ma, R. Yang, H. Li, M. Ma, B. Ren, N. Popovic, N. Sebe, E. Konukoglu, T. Gevers *et al.*, "Scenesplat: Gaussian splatting-based scene understanding with vision-language pretraining," in *ICCV*, 2025.
- [122] T. Brooks, A. Holynski, and A. A. Efros, "Instructpix2pix: Learning to follow image editing instructions," in *CVPR*, 2023.
- [123] Y. Yang, Y. Wang, T. Zhang, J. Wang, and S. He, "Prompt-softbox-prompt: A free-text embedding control for image editing," in *ACM MM*, 2025.
- [124] D. I. Lee, H. Park, J. Seo, E. Park, H. Park, H. D. Baek, S. Sangheon, S. Kim *et al.*, "Editsplat: Multi-view fusion and attention-guided optimization for view-consistent 3d scene editing with 3d gaussian splatting," in *CVPR*, 2025.
- [125] F. Palandra, A. Sanchietti, D. Baieri, and E. Rodolà, "Gsedit: Efficient text-guided editing of 3d objects via gaussian splatting," *arXiv preprint arXiv:2403.05154*, 2024.
- [126] Y. Huang, B. Liao, Y. Hu, H. Lin, L. Wu, S. Li, C. Tan, Z. Liu, Y. Liu, Z. Zang *et al.*, "Dacapo: Score distillation as stacked bridge for fast and high-quality 3d editing," in *CVPR*, 2025.
- [127] Y. Sun, R. Tian, X. Han, X. Liu, Y. Zhang, and K. Xu, "Gseditpro: 3d gaussian splatting editing with attention-based progressive localization," in *Computer Graphics Forum*, 2024.
- [128] N. Ruiz, Y. Li, V. Jampani, Y. Pritch, M. Rubinstein, and K. Aberman, "Dreambooth: Fine tuning text-to-image diffusion models for subject-driven generation," in *CVPR*, 2023.
- [129] H. Xiao, Y. Chen, H. Huang, H. Xiong, J. Yang, P. Prasad, and Y. Zhao, "Localized gaussian splatting editing with contextual awareness," in *WACV*, 2025.
- [130] J. Wu, J.-W. Bian, X. Li, G. Wang, I. Reid, P. Torr, and V. A. Prisacariu, "Gaussctrl: Multi-view consistent text-driven 3d gaussian splatting editing," in *ECCV*, 2024.
- [131] C. Luo, D. Di, X. Yang, Y. Ma, Z. Xue, C. Wei, and Y. Liu, "Trame: Trajectory-anchored multi-view editing for text-guided 3d gaussian splatting manipulation," *IEEE TMM*, 2025.
- [132] E. Gomel and L. Wolf, "Diffusion-based attention warping for consistent 3d scene editing," *arXiv preprint arXiv:2412.07984*, 2024.
- [133] M. Chen, I. Laina, and A. Vedaldi, "Dge: Direct gaussian 3d editing by consistent multi-view editing," in *ECCV*, 2024.
- [134] H. Go, B. Park, J. Jang, J.-Y. Kim, S. Kwon, and C. Kim, "Splatflow: Multi-view rectified flow model for 3d gaussian splatting synthesis," in *CVPR*, 2025.
- [135] M. Wen, S. Wu, K. Wang, and D. Liang, "Intergsedit: Interactive 3d gaussian splatting editing with 3d geometry-consistent attention prior," in *ICCV*, 2025.
- [136] Y. Zhao, W. Xu, Y. Wu, W. Huang, Z. Sun, and W. Yang, "Progdf: Progressive gaussian differential field for controllable and flexible 3d editing," *arXiv preprint arXiv:2412.08152*, 2024.
- [137] Z. Yan, L. Li, Y. Shao, S. Chen, W. Kai, J.-N. Hwang, H. Zhao, and F. Remondino, "3dsceneeditor: Controllable 3d scene editing with gaussian splatting," *arXiv preprint arXiv:2412.01583*, 2024.
- [138] Q. Zhang, Y. Xu, C. Wang, H.-Y. Lee, G. Wetzstein, B. Zhou, and C. Yang, "3ditscene: Editing any scene via language-guided disentangled gaussian splatting," in *ICLR*, 2025.
- [139] Y. Wang, Q. Wu, G. Zhang, and D. Xu, "Learning 3d geometry and feature consistent gaussian splatting for object removal," in *ECCV*, 2024.
- [140] J. Waczynska, P. Borycki, J. Kaleta, S. Tadeja, and P. Spurek, "D-miso: Editing dynamic 3d scenes using multi-gaussians soup," *NeurIPS*, 2024.
- [141] T.-X. Xu, W. Hu, Y.-K. Lai, Y. Shan, and S.-H. Zhang, "Texture-gs: Disentangling the geometry and texture for 3d gaussian splatting editing," in *ECCV*, 2024.
- [142] K. He, C.-H. Wu, and I. Gilitschenski, "Ctrl-d: Controllable dynamic 3d scene editing with personalized 2d diffusion," in *CVPR*, 2025.
- [143] E. J. Hu, Y. Shen, P. Wallis, Z. Allen-Zhu, Y. Li, S. Wang, L. Wang, and W. Chen, "Lora: Low-rank adaptation of large language models," in *ICLR*, 2022.
- [144] Y. Cao, M. Hadi, L. Pan, and Z. Liu, "Gs-vton: Controllable 3d virtual try-on with gaussian splatting," *arXiv preprint arXiv:2410.05259*, 2024.
- [145] H. Cha, I. Lee, and H. Joo, "Perse: Personalized 3d generative avatars from a single portrait," *arXiv preprint arXiv:2412.21206*, 2024.
- [146] T. Xu, P. Chen, Jiamin an d Chen, Y. Zhang, J. Yu, and W. Yang, "Tiger: Text-instructed 3d gaussian retrieval and coherent editing," *arXiv preprint arXiv:2405.14455*, 2024.
- [147] J. Huang, H. Yu, J. Zhang, and H. Nait-Charif, "Point'n move: Interactive scene object manipulation on gaussian splatting radiance fields," *IET Image Processing*, 2024.
- [148] J. Szymkowiak, W. Jakubowska, D. Malarz, W. Smolak-Dyżewska, M. Zięba, P. Musiański, W. Pałubicki, and P. Spurek, "Neural surface priors for editable gaussian splatting," *arXiv*, 2024.
- [149] H. Chen, Y. Huang, H. Huang, X. Ge, and D. Shao, "Gaussianvton: 3d human virtual try-on via multi-stage gaussian splatting editing with image prompting," *arXiv preprint arXiv:2405.07472*, 2024.
- [150] B. Galerne, J. Wang, L. Raad, and J.-M. Morel, "Sgsst: Scaling gaussian splatting styletransfer," in *CVPR*, 2025.
- [151] Y. Mei, J. Xu, and V. Patel, "Regs: Reference-based controllable scene stylization with gaussian splatting," *NeurIPS*, 2024.
- [152] D. Kotovenko, O. Grebenkova, N. Sarafianos, A. Paliwal, P. Ma, O. Poursaeed, S. Mohan, Y. Fan, Y. Li, R. Ranjan *et al.*, "Wast-3d: Wasserstein-2 distance for scene-to-scene stylization on 3d gaussians," in *ECCV*, 2024.
- [153] Y. Lin, J. Lei, and K. Jia, "Multi-stylegs: Stylized gaussian splatting with multiple styles," in *AAAI*, 2025.
- [154] X.-Y. Yu, J.-X. Yu, L.-B. Zhou, Y. Wei, and L.-L. Ou, "Instantstyle-gaussian: Efficient art style transfer with 3d gaussian splatting," *arXiv preprint arXiv:2408.04249*, 2024.
- [155] Z. Gu, Z. Zhang, M. Li, Z. Ji, R. Chen, Z. Hu, and G. Ye, "Artnvg: Content-style separated artistic neighboring-view gaussian stylization," in *ICMR*, 2025.
- [156] J. Wynn, Z. Qureshi, J. Powierza, J. Watson, and M. Sayed, "Morpheus: Text-driven 3d gaussian splat shape and color stylization," in *CVPR*, 2025.
- [157] Y. Yang, Y. Wang, C. Wang, H. Wang, and S. He, "Fantasystyle: Controllable stylized distillation for 3d gaussian splatting," *arXiv*, 2025.
- [158] A. Saroha, M. Gladkova, C. Curreli, D. Muhle, T. Yenamandra, and D. Cremers, "Gaussian splatting in style," *arXiv:2403.08498*, 2024.

- [159] S. Jain, A. Kuthiala, P. S. Sethi, and P. Saxena, “Stylesplat: 3d object style transfer with gaussian splatting,” *arXiv:2407.09473*, 2024.
- [160] K. Liu, F. Zhan, M. Xu, C. Theobalt, L. Shao, and S. Lu, “Stylegaussian: Instant 3d style transfer with gaussian splatting,” in *SIGGRAPH Asia*, 2024.
- [161] S. N. Sinha, H. Graf, and M. Weinmann, “Semanticsplatstylization: Semantic scene stylization based on 3d gaussian splatting and class-based style transfer,” in *GCH*, 2024.
- [162] R.-Z. Qiu, G. Yang, W. Zeng, and X. Wang, “Language-driven physics-based scene synthesis and editing via feature splatting,” in *ECCV*, 2024.
- [163] H. Chen, Y. Lan, Y. Chen, Y. Zhou, and X. Pan, “Mvdrag3d: Drag-based creative 3d editing via multi-view generation-reconstruction priors,” *arXiv preprint arXiv:2410.16272*, 2024.
- [164] Y. Qu, D. Chen, X. Li, X. Li, S. Zhang, L. Cao, and R. Ji, “Drag your gaussian: Effective drag-based editing with score distillation for 3d gaussian splatting,” *arXiv preprint arXiv:2501.18672*, 2025.
- [165] U. Khalid, H. Iqbal, A. Farooq, J. Hua, and C. Chen, “3dego: 3d editing on the go!” in *ECCV*, 2024.
- [166] X. Gao, H. Xiao, C. Zhong, S. Hu, Y. Guo, and J. Zhang, “Portrait video editing empowered by multimodal generative priors,” in *SIGGRAPH Asia*, 2024.
- [167] Z. Liu, H. Ouyang, Q. Wang, K. L. Cheng, J. Xiao, K. Zhu, N. Xue, Y. Liu, Y. Shen, and Y. Cao, “Infusion: Inpainting 3d gaussians via learning depth completion from diffusion prior,” *arXiv preprint arXiv:2404.11613*, 2024.
- [168] A. Mirzaei, R. De Lutio, S. W. Kim, D. Acuna, J. Kelly, S. Fidler, I. Gilitschenski, and Z. Gojcic, “Reffusion: Reference adapted diffusion models for 3d scene inpainting,” *arXiv preprint arXiv:2404.10765*, 2024.
- [169] W. Wang and Y. Fu, “Text-to-3d gaussian splatting with physics-grounded motion generation,” *arXiv preprint arXiv:2412.05560*, 2024.
- [170] X. Yang and X. Wang, “Hash3d: Training-free acceleration for 3d generation,” in *CVPR*, 2025.
- [171] Y. Zhou, Z. He, Q. Li, and C. Wang, “Layoutdreamer: Physics-guided layout for text-to-3d compositional scene generation,” *arXiv preprint arXiv:2502.01949*, 2025.
- [172] L. Qiu, G. Chen, X. Gu, Q. Zuo, M. Xu, Y. Wu, W. Yuan, Z. Dong, L. Bo, and X. Han, “Richdreamer: A generalizable normal-depth diffusion model for detail richness in text-to-3d,” in *CVPR*, 2024.
- [173] Z. Chen, F. Wang, Y. Wang, and H. Liu, “Text-to-3d using gaussian splatting,” in *CVPR*, 2024.
- [174] T. Yi, J. Fang, Z. Zhou, J. Wang, G. Wu, L. Xie, X. Zhang, W. Liu, X. Wang, and Q. Tian, “Gaussiandreamerpro: Text to manipulable 3d gaussians with highly enhanced quality,” *arXiv preprint arXiv:2406.18462*, 2024.
- [175] C. Ge, C. Xu, Y. Ji, C. Peng, M. Tomizuka, P. Luo, M. Ding, V. Jampani, and W. Zhan, “Compgs: Unleashing 2d compositionality for compositional text-to-3d via dynamically optimizing 3d gaussians,” *arXiv preprint arXiv:2410.20723*, 2024.
- [176] A. Vilesov, P. Chari, and A. Kadambi, “Cg3d: Compositional generation for text-to-3d via gaussian splatting,” *arXiv preprint arXiv:2311.17907*, 2023.
- [177] D. Di, J. Yang, C. Luo, Z. Xue, W. Chen, X. Yang, and Y. Gao, “Hyper-3dg: Text-to-3d gaussian generation via hypergraph,” *IJCV*, 2025.
- [178] Y. Qin, Z. Xu, and Y. Liu, “Apply hierarchical-chain-of-generation to complex attributes text-to-3d generation,” in *CVPR*, 2025.
- [179] S. Chen, J. Zhou, Z. Jiang, T. Zhang, Z. Wu, J.-N. Hwang, and L. Li, “Scalinggaussian: Enhancing 3d content creation with generative gaussian splatting,” *arXiv preprint arXiv:2407.19035*, 2024.
- [180] F. Liu, H. Wang, S. Yao, S. Zhang, J. Zhou, and Y. Duan, “Physics3d: Learning physical properties of 3d gaussians via video diffusion,” *arXiv preprint arXiv:2406.04338*, 2024.
- [181] P. Guo, H. Hao, A. Caccavale, Z. Ren, E. Zhang, Q. Shan, A. Sankar, A. G. Schwing, A. Colburn, and F. Ma, “Stabledreamer: taming noisy score distillation sampling for text-to-3d,” *arXiv preprint arXiv:2312.02189*, 2023.
- [182] Z. Li, M. Hu, Q. Zheng, and X. Jiang, “Connecting consistency distillation to score distillation for text-to-3d generation,” in *ECCV*, 2024.
- [183] Z. Cai, D. Wang, Y. Liang, Z. Shao, Y.-C. Chen, X. Zhan, and Z. Wang, “Dreammapping: High-fidelity text-to-3d generation via variational distribution mapping,” *arXiv preprint arXiv:2409.05099*, 2024.
- [184] X. Liu, X. Zhan, J. Tang, Y. Shan, G. Zeng, D. Lin, X. Liu, and Z. Liu, “Humangaussian: Text-driven 3d human generation with gaussian splatting,” in *CVPR*, 2024.
- [185] X. Miao, H. Duan, V. Ojha, J. Song, T. Shah, Y. Long, and R. Ranjan, “Dreamer xl: Towards high-resolution text-to-3d generation via trajectory score matching,” *arXiv preprint arXiv:2405.11252*, 2024.
- [186] J. Song, C. Meng, and S. Ermon, “Denoising diffusion implicit models,” *arXiv preprint arXiv:2010.02502*, 2020.
- [187] G. Shim, S. Lee, and J. Choo, “Gaussianmotion: End-to-end learning of animatable gaussian avatars with pose guidance from text,” *arXiv preprint arXiv:2502.11642*, 2025.
- [188] H. Basak, H. Tabatabaee, S. Gayaka, M.-F. Li, X. Yang, C.-H. Kuo, A. Sen, M. Sun, and Z. Yin, “Enhancing single image to 3d generation using gaussian splatting and hybrid diffusion priors,” *arXiv preprint arXiv:2410.09467*, 2024.
- [189] C. Wang, J. Gu, X. Long, Y. Liu, and L. Liu, “Geco: Generative image-to-3d within a second,” *arXiv preprint arXiv:2405.20327*, 2024.
- [190] Z. Wang, C. Lu, Y. Wang, F. Bao, C. Li, H. Su, and J. Zhu, “Prolificdreamer: High-fidelity and diverse text-to-3d generation with variational score distillation,” *NeurIPS*, 2023.
- [191] T. Huang, H. Zhang, Y. Zeng, Z. Zhang, H. Li, W. Zuo, and R. W. Lau, “Dreamphysics: Learning physical properties of dynamic 3d gaussians with video diffusion priors,” *arXiv preprint arXiv:2406.01476*, 2024.
- [192] P. Pham, A. N. Mathur, O. Sharma, and A. Bera, “Mygaussian: High-fidelity text-to-3d content generation with multi-view guidance and surface densification,” *arXiv preprint arXiv:2409.06620*, 2024.
- [193] T. Ukarapol and K. Pruvost, “Gradeadreamer: Enhanced text-to-3d generation using gaussian splatting and multi-view diffusion,” *arXiv preprint arXiv:2406.09850*, 2024.
- [194] X. Zhou, X. Ran, Y. Xiong, J. He, Z. Lin, Y. Wang, D. Sun, and M.-H. Yang, “GALA3d: Towards text-to-3d complex scene generation via layout-guided generative gaussian splatting,” in *ICML*, 2024.
- [195] Y. Shi, P. Wang, J. Ye, L. Mai, K. Li, and X. Yang, “MVDream: Multi-view diffusion for 3d generation,” in *ICLR*, 2024.
- [196] Z. Li, Y. Chen, L. Zhao, and P. Liu, “Controllable text-to-3d generation via surface-aligned gaussian splatting,” *arXiv preprint arXiv:2403.09981*, 2024.
- [197] J. Han, F. Kokkinos, and P. Torr, “Vfusion3d: Learning scalable 3d generative models from video diffusion models,” in *ECCV*, 2024.
- [198] X. He, J. Chen, S. Peng, D. Huang, Y. Li, X. Huang, C. Yuan, W. Ouyang, and T. He, “Gvgen: Text-to-3d generation with xxvolumetric representation,” in *ECCV*, 2024.
- [199] S. Wizadwongsa, J. Zhou, E. Li, and J. J. Park, “Taming feed-forward reconstruction models as latent encoders for 3d generative models,” *arXiv preprint arXiv:2501.00651*, 2024.
- [200] L. Yushi, S. Zhou, Z. Lyu, F. Hong, S. Yang, B. Dai, X. Pan, and C. C. Loy, “Gaussiananything: Interactive point cloud flow matching for 3d generation,” in *ICLR*, 2025.
- [201] H. Yang, Y. Dong, H. Jiang, D. Xu, G. Pavlakos, and Q. Huang, “Atlas gaussians diffusion for 3d generation,” in *ICLR*, 2025.
- [202] H. Hu, T. Yin, F. Luan, Y. Hu, H. Tan, Z. Xu, S. Bi, S. Tulsiani, and K. Zhang, “Turbo3d: Ultra-fast text-to-3d generation,” in *CVPR*, 2025.
- [203] D. Xu, Y. Yuan, M. Mardani, S. Liu, J. Song, Z. Wang, and A. Vahdat, “AGG: Amortized generative 3d gaussians for single image to 3d,” *TMLR*, 2024.
- [204] P. Pan, Z. Su, C. Lin, Z. Fan, Y. Zhang, Z. Li, T. Shen, Y. Mu, and Y. Liu, “Humansplat: Generalizable single-image human gaussian splatting with structure priors,” *NeurIPS*, 2024.
- [205] Z.-X. Zou, Z. Yu, Y.-C. Guo, Y. Li, D. Liang, Y.-P. Cao, and S.-H. Zhang, “Triplane meets gaussian splatting: Fast and generalizable single-view 3d reconstruction with transformers,” in *CVPR*, 2024.
- [206] J. Han, J. Wang, A. Vedaldi, P. Torr, and F. Kokkinos, “Flex3d: Feed-forward 3d generation with flexible reconstruction model and input view curation,” *arXiv preprint arXiv:2410.00890*, 2024.
- [207] Q. Feng, Z. Xing, Z. Wu, and Y.-G. Jiang, “Geogs3d: Single-view 3d reconstruction via geometric-aware diffusion model and gaussian splatting,” *arXiv preprint arXiv:2403.10242*, 2024.
- [208] L. Jiang and L. Wang, “Brightdreamer: Generic 3d gaussian generative framework for fast text-to-3d synthesis,” *arXiv preprint arXiv:2403.11273*, 2024.
- [209] L. Lu, H. Gao, T. Dai, Y. Zha, Z. Hou, J. Wu, and S.-T. Xia, “Large point-to-gaussian model for image-to-3d generation,” in *ACM MM*, 2024.
- [210] J. Wu, K. Liu, Y. Shi, X. Jiang, Y. Yao, and L. Zhang, “Unigs: Modeling unitary 3d gaussians for novel view synthesis from sparse-view images,” in *ICCV*, 2025.
- [211] J. Liu, J. Xu, W. Cheng, Y. Gao, X. Wang, Y. Shan, and Y. Tang, “Novelgels: Consistent novel-view denoising via large gaussian reconstruction model,” *arXiv preprint arXiv:2411.16779*, 2024.

- [212] H. Wen, Z. Huang, Y. Wang, X. Chen, and L. Sheng, "Ouroboros3d: Image-to-3d generation via 3d-aware recursive diffusion," in *CVPR*, 2025.
- [213] Z. Tang, J. Zhang, X. Cheng, W. Yu, C. Feng, Y. Pang, B. Lin, and L. Yuan, "Cycle3d: High-quality and consistent image-to-3d generation via generation-reconstruction cycle," in *AAAI*, 2025.
- [214] Y. Cai, H. Zhang, K. Zhang, Y. Liang, M. Ren, F. Luan, Q. Liu, S. Y. Kim, J. Zhang, Z. Zhang *et al.*, "Baking gaussian splatting into diffusion denoiser for fast and scalable single-stage image-to-3d generation," in *ICCV*, 2025.
- [215] H. Yang, Y. Chen, Y. Pan, T. Yao, Z. Chen, C.-W. Ngo, and T. Mei, "Hi3d: Pursuing high-resolution image-to-3d generation with video diffusion models," in *ACM MM*, 2024.
- [216] X. Yu, Y.-C. Guo, Y. Li, D. Liang, S.-H. Zhang, and X. QI, "Text-to-3d with classifier score distillation," in *ICLR*, 2024.
- [217] Y. Ma, D. Zhan, and Z. Jin, "Fastscene: Text-driven fast 3d indoor scene generation via panoramic gaussian splatting," in *IJCAI*, 2024.
- [218] Y. Zhong, Z. Li, D. Z. Chen, L. Hong, and D. Xu, "Taming video diffusion prior with scene-grounding guidance for 3d gaussian splatting from sparse inputs," in *CVPR*, 2025.
- [219] H.-X. Yu, H. Duan, C. Herrmann, W. T. Freeman, and J. Wu, "Wonderworld: Interactive 3d scene generation from a single image," in *CVPR*, 2025.
- [220] Z. Huang, J. He, J. Ye, L. Jiang, W. Li, Y. Chen, and T. Han, "Scene4u: Hierarchical layered 3d scene reconstruction from single panoramic image for your immerse exploration," in *CVPR*, 2025.
- [221] H. Ouyang, K. Heal, S. Lombardi, and T. Sun, "Text2immersion: Generative immersive scene with 3d gaussians," *arXiv*, 2023.
- [222] J. Shriram, A. Trevisan, L. Liu, and R. Ramamoorthi, "Realdreamer: Text-driven 3d scene generation with inpainting and depth diffusion," *3DV*, 2025.
- [223] H.-X. Yu, H. Duan, J. Hur, K. Sargent, M. Rubinstein, W. T. Freeman, F. Cole, D. Sun, N. Snavely, J. Wu *et al.*, "Wonderjourney: Going from anywhere to everywhere," in *CVPR*, 2024.
- [224] H. Zhou, X. Cheng, W. Yu, Y. Tian, and L. Yuan, "Holodreamer: Holistic 3d panoramic world generation from text descriptions," *arXiv preprint arXiv:2407.15187*, 2024.
- [225] J. Chung, S. Lee, H. Nam, J. Lee, and K. M. Lee, "Luciddreamer: Domain-free generation of 3d gaussian splatting scenes," *arXiv preprint arXiv:2311.13384*, 2023.
- [226] H. Wang, Y. Liu, Z. Liu, W. Wang, Z. Dong, and B. Yang, "Vistadream: Sampling multiview consistent images for single-view scene reconstruction," in *ICCV*, 2025.
- [227] X. Kang, Z. Xiang, Z. Zhang, and K. Khoshelham, "Multi-view geometry-aware diffusion transformer for indoor novel view synthesis," in *ICLR*, 2025.
- [228] Z. Wu, H. Xu, G. Xu, P. Nie, Z. Yan, J. Zheng, L. Qu, M. Li, and L. Nie, "Textsplat: Text-guided semantic fusion for generalizable gaussian splatting," *arXiv preprint arXiv:2504.09588*, 2025.
- [229] D. Charatan, S. L. Li, A. Tagliasacchi, and V. Sitzmann, "pixelsplat: 3d gaussian splats from image pairs for scalable generalizable 3d reconstruction," in *CVPR*, 2024.
- [230] Z. Chen, C. Wu, Z. Shen, C. Zhao, W. Ye, H. Feng, E. Ding, and S.-H. Zhang, "Splat360: Generalizable 360 gaussian splatting for wide-baseline panoramic images," in *CVPR*, 2025.
- [231] Y. Chen, C. Zheng, H. Xu, B. Zhuang, A. Vedaldi, T.-J. Cham, and J. Cai, "Mvsplat360: Feed-forward 360 scene synthesis from sparse views," in *NeurIPS*, 2024.
- [232] H. Xie, Z. Chen, F. Hong, and Z. Liu, "Generative gaussian splatting for unbounded 3d city generation," in *CVPR*, 2025.
- [233] G. Kang, J. Yoo, J. Park, S. Nam, H. Im, S. Shin, S. Kim, and E. Park, "Selfsplat: Pose-free and 3d prior-free generalizable 3d gaussian splatting," in *CVPR*, 2025.
- [234] W. Roh, H. Jung, J. W. Kim, S. Lee, I. Yoo, A. Lugmayr, S. Chi, K. Ramani, and S. Kim, "Catsplat: Context-aware transformer with spatial guidance for generalizable 3d gaussian splatting from a single-view image," in *ICCV*, 2025.
- [235] S. Lee, J. Chung, K. Kim, J. Huh, G. Lee, M. Lee, and K. M. Lee, "Omnisplat: Taming feed-forward 3d gaussian splatting for omnidirectional images with editable capabilities," in *CVPR*, 2025.
- [236] Y. Yang, J. Shao, X. Li, Y. Shen, A. Geiger, and Y. Liao, "Prometheus: 3d-aware latent diffusion models for feed-forward text-to-3d scene generation," in *CVPR*, 2025.
- [237] H. Go, B. Park, H. Nam, B.-H. Kim, H. Chung, and C. Kim, "Videorf-splat: Direct scene-level text-to-3d gaussian splatting generation with flexible pose and multi-view joint modeling," in *ICCV*, 2025.
- [238] W. Yu, J. Xing, L. Yuan, W. Hu, X. Li, Z. Huang, X. Gao, T.-T. Wong, Y. Shan, and Y. Tian, "Viewcrafter: Taming video diffusion models for high-fidelity novel view synthesis," *arXiv preprint arXiv:2409.02048*, 2024.
- [239] H. Liang, J. Cao, V. Goel, G. Qian, S. Korolev, D. Terzopoulos, K. N. Plataniotis, S. Tulyakov, and J. Ren, "Wonderland: Navigating 3d scenes from a single image," in *CVPR*, 2025.
- [240] K. Schwarz, N. Mueller, and P. Kotschieder, "Generative gaussian splatting: Generating 3d scenes with video diffusion priors," in *ICCV*, 2025.
- [241] H. Wang, F. Liu, J. Chi, and Y. Duan, "Videoscene: Distilling video diffusion model to generate 3d scenes in one step," in *CVPR*, 2025.
- [242] S. Zhang, J. Li, X. Fei, H. Liu, and Y. Duan, "Scene splatter: Momentum 3d scene generation from single image with video diffusion model," in *CVPR*, 2025.
- [243] Z. Li, Z. Zheng, L. Wang, and Y. Liu, "Animatable gaussians: Learning pose-dependent gaussian maps for high-fidelity human avatar modeling," in *CVPR*, 2024.
- [244] Y. Jiang, Z. Shen, P. Wang, Z. Su, Y. Hong, Y. Zhang, J. Yu, and L. Xu, "Hifi4g: High-fidelity human performance rendering via compact gaussian splatting," in *CVPR*, 2024.
- [245] J. Chen, "Ggavatar: Reconstructing garment-separated 3d gaussian splatting avatars from monocular video," in *ACM MM*, 2024.
- [246] J. Chen, J. Hu, G. Wang, Z. Jiang, T. Zhou, Z. Chen, and C. Lv, "Taoavatar: Real-time lifelike full-body talking avatars for augmented reality via 3d gaussian splatting," in *CVPR*, 2025.
- [247] M. Kocabas, J.-H. R. Chang, J. Gabriel, O. Tuzel, and A. Ranjan, "Hugs: Human gaussian splats," in *CVPR*, 2024.
- [248] R. Abdal, W. Yifan, Z. Shi, Y. Xu, R. Po, Z. Kuang, Q. Chen, D.-Y. Yeung, and G. Wetzstein, "Gaussian shell maps for efficient 3d human generation," in *CVPR*, 2024.
- [249] M. Loper, N. Mahmood, J. Romero, G. Pons-Moll, and M. J. Black, "Smpl: A skinned multi-person linear model," *ACM TOG*, 2023.
- [250] G. Pavlakos, V. Choutas, N. Ghorbani, T. Bolkart, A. A. Osman, D. Tzionas, and M. J. Black, "Expressive body capture: 3d hands, face, and body from a single image," in *CVPR*, 2019.
- [251] W. Zielonka, T. Bagautdinov, S. Saito, M. Zollhöfer, J. Thies, and J. Romero, "Drivable 3d gaussian avatars," in *3DV*, 2025.
- [252] S. Hu, T. Hu, and Z. Liu, "Gauhuman: Articulated gaussian splatting from monocular human videos," in *CVPR*, 2024.
- [253] W.-Q. Feng, D. Han, Z.-K. Zhou, S. Li, X. Liu, P. Wan, D. Zhang, and M. Wang, "Gpavatar: High-fidelity head avatars by learning efficient gaussian projections," in *CVPR*, 2025.
- [254] D. Zhang, Y. Liu, L. Lin, Y. Zhu, K. Chen, M. Qin, Y. Li, and H. Wang, "Hravatar: High-quality and relightable gaussian head avatar," in *CVPR*, 2025.
- [255] X. Sun, Z. Cai, Y. Tai, J. Yang, and Z. Zhang, "Strandhead: Text to hair-disentangled 3d head avatars using human-centric priors," in *ICCV*, 2025.
- [256] T. Li, T. Bolkart, M. J. Black, H. Li, and J. Romero, "Learning a model of facial shape and expression from 4d scans," *ACM TOG*, 2017.
- [257] Y. Xu, B. Chen, Z. Li, H. Zhang, L. Wang, Z. Zheng, and Y. Liu, "Gaussian head avatar: Ultra high-fidelity head avatar via dynamic gaussians," in *CVPR*, 2024.
- [258] R. B. Li, M. Shaghagh, K. Suzuki, X. Liu, V. Mopathi, B. Du, W. Curtis, M. Renschler, K. M. B. Lee, N. Atanasov *et al.*, "Dynaglam: Real-time gaussian-splatting slam for online rendering, tracking, motion predictions of moving objects in dynamic scenes," in *ICCV*, 2025.
- [259] C. Cheng, S. Yu, Z. Wang, Y. Zhou, and H. Wang, "Outdoor monocular slam with global scale-consistent 3d gaussian pointmaps," in *ICCV*, 2025.
- [260] Y. F. Tianci Wen, Zhiang Liu, "Segs-slam: Structure-enhanced 3d gaussian splatting slam with appearance embedding," in *ICCV*, 2025.
- [261] J. Zheng, Z. Zhu, V. Bieri, M. Pollefeys, S. Peng, and I. Armeni, "Wildgs-slam: Monocular gaussian splatting slam in dynamic environments," in *CVPR*, 2025.
- [262] N. Keetha, J. Karhade, K. M. Jatavallabhula, G. Yang, S. Scherer, D. Ramanan, and J. Luiten, "Splatmap: Splat track & map 3d gaussians for dense rgb-d slam," in *CVPR*, 2024.
- [263] H. Matsuki, R. Murai, P. H. Kelly, and A. J. Davison, "Gaussian splatting slam," in *CVPR*, 2024.
- [264] H. Huang, L. Li, H. Cheng, and S.-K. Yeung, "Photo-slam: Real-time simultaneous localization and photorealistic mapping for monocular stereo and rgb-d cameras," in *CVPR*, 2024.
- [265] M. Li, S. Liu, H. Zhou, G. Zhu, N. Cheng, T. Deng, and H. Wang, "Sgs-slam: Semantic gaussian splatting for neural dense slam," in *ECCV*, 2024.

- [266] D. Yang, Y. Gao, X. Wang, Y. Yue, Y. Yang, and M. Fu, “Opengs-slam: Open-set dense semantic slam with 3d gaussian splatting for object-level scene understanding,” in *ICRA*, 2025.
- [267] L. Li, L. Zhang, Z. Wang, and Y. Shen, “Gs3lam: Gaussian semantic splatting slam,” in *ACM MM*, 2024.
- [268] J. Yu, K. Hari, K. Srinivas, K. El-Refai, A. Rashid, C. M. Kim, J. Kerr, R. Cheng, M. Z. Irshad, A. Balakrishna *et al.*, “Language-embedded gaussian splats (legs): Incrementally building room-scale representations with a mobile robot,” in *IROS*, 2024.
- [269] Z. Liu, S. Zheng, S. Chen, C. Zhao, L. Liang, X. Xue, and Y. Fu, “A neural representation framework with llm-driven spatial reasoning for open-vocabulary 3d visual grounding,” in *ACM MM*, 2025.
- [270] H. Yan, Y. Zheng, and Y. Duan, “Gaussian-det: Learning closed-surface gaussians for 3d object detection,” in *ICLR*, 2024.
- [271] Y. Cao, Y. Jv, and D. Xu, “3dgs-det: Empower 3d gaussian splatting with boundary guidance and box-focused sampling for 3d object detection,” *arXiv preprint arXiv:2410.01647*, 2024.
- [272] J. W. Lee, H. Lim, S. Yang, and J. B. Choi, “Matt-gs: Masked attention-based 3dgs for robot perception and object detection,” in *IROS*, 2025.
- [273] S. Widadwongsa, P. Phongthawee, J. Yenphraphai, and S. Suwanajakorn, “Nex: Real-time view synthesis with neural basis expansion,” in *CVPR*, 2021.
- [274] A. Dai, A. X. Chang, M. Savva, M. Halber, T. Funkhouser, and M. Nießner, “ScanNet: Richly-annotated 3d reconstructions of indoor scenes,” in *CVPR*, 2017.
- [275] J. T. Barron, B. Mildenhall, D. Verbin, P. P. Srinivasan, and P. Hedman, “Mip-nerf 360: Unbounded anti-aliased neural radiance fields,” in *CVPR*, 2022.
- [276] M. Deitke, D. Schwenk, J. Salvador, L. Weihs, O. Michel, E. VanderBilt, L. Schmidt, K. Ehsani, A. Kembhavi, and A. Farhadi, “Objaverse: A universe of annotated 3d objects,” in *CVPR*, 2023.
- [277] L. Downs, A. Francis, N. Koenig, B. Kinman, R. Hickman, K. Reymann, T. B. McHugh, and V. Vanhoucke, “Google scanned objects: A high-quality dataset of 3d scanned household items,” in *ICRA*, 2022.
- [278] A. X. Chang, T. Funkhouser, L. Guibas, P. Hanrahan, Q. Huang, Z. Li, S. Savarese, M. Savva, S. Song, H. Su *et al.*, “Shapenet: An information-rich 3d model repository,” *arXiv preprint arXiv:1512.03012*, 2015.
- [279] J. Straub, T. Whelan, L. Ma, Y. Chen, E. Wijmans, S. Green, J. J. Engel, R. Mur-Artal, C. Ren, S. Verma *et al.*, “The replica dataset: A digital replica of indoor spaces,” *arXiv preprint arXiv:1906.05797*, 2019.
- [280] M. Ma, Q. Ma, Y. Li, J. Cheng, R. Yang, B. Ren, N. Popovic, M. Wei, N. Sebe, L. Van Gool *et al.*, “Scenesplat++: A large dataset and comprehensive benchmark for language gaussian splatting,” *arXiv preprint arXiv:2506.08710*, 2025.
- [281] Z. Ren, A. Agarwala, B. Russell, A. G. Schwing, and O. Wang, “Neural volumetric object selection,” in *CVPR*, 2022.
- [282] H. Ding, S. Tang, S. He, C. Liu, Z. Wu, and Y.-G. Jiang, “Multimodal referring segmentation: A survey,” *arXiv preprint arXiv:2508.00265*, 2025.
- [283] C. Liu, H. Ding, and X. Jiang, “GRES: Generalized referring expression segmentation,” in *CVPR*, 2023.
- [284] Y. Shen, C. Fu, P. Chen, M. Zhang, K. Li, X. Sun, Y. Wu, S. Lin, and R. Ji, “Aligning and prompting everything all at once for universal visual perception,” in *CVPR*, 2024.
- [285] R. Zhu, M. Yu, L. Xu, L. Jiang, Y. Li, T. Zhang, J. Pang, and B. Dai, “Objectgs: Object-aware scene reconstruction and scene understanding via gaussian splatting,” in *ICCV*, 2025.
- [286] R. Jensen, A. Dahl, G. Vogiatzis, E. Tola, and H. Aanaes, “Large scale multi-view stereopsis evaluation,” in *CVPR*, 2014.
- [287] A. Knapitsch, J. Park, Q.-Y. Zhou, and V. Koltun, “Tanks and temples: Benchmarking large-scale scene reconstruction,” *ACM TOG*, 2017.
- [288] T. Shen, Z. Luo, L. Zhou, R. Zhang, S. Zhu, T. Fang, and L. Quan, “Matchable image retrieval by learning from surface reconstruction,” in *ACCV*, 2018.
- [289] B. Mildenhall, P. P. Srinivasan, R. Ortiz-Cayon, N. K. Kalantari, R. Ramamoorthi, R. Ng, and A. Kar, “Local light field fusion: Practical view synthesis with prescriptive sampling guidelines,” *ACM TOG*, 2019.
- [290] Y. Yao, Z. Luo, S. Li, J. Zhang, Y. Ren, L. Zhou, T. Fang, and L. Quan, “Blendedmvs: A large-scale dataset for generalized multi-view stereo networks,” in *CVPR*, 2020.
- [291] J. Reizenstein, R. Shapovalov, P. Henzler, L. Sbordone, P. Labatut, and D. Novotny, “Common objects in 3d: Large-scale learning and evaluation of real-life 3d category reconstruction,” in *ICCV*, 2021.
- [292] M. Tancik, E. Weber, E. Ng, R. Li, B. Yi, T. Wang, A. Kristoffersen, J. Austin, K. Salahi, A. Ahuja *et al.*, “Nerfstudio: A modular framework for neural radiance field development,” in *ACM SIGGRAPH*, 2023.
- [293] C. Yeshwanth, Y.-C. Liu, M. Nießner, and A. Dai, “ScanNet++: A high-fidelity dataset of 3d indoor scenes,” in *ICCV*, 2023.
- [294] C.-H. Wu, Y.-J. Chen, Y.-H. Chen, J.-Y. Lee, B.-H. Ke, C.-W. T. Mu, Y.-C. Huang, C.-Y. Lin, M.-H. Chen, Y.-Y. Lin *et al.*, “Aurafusion360: Augmented unseen region alignment for reference-based 360deg unbounded scene inpainting,” in *CVPR*, 2025.
- [295] C. Szegedy, V. Vanhoucke, S. Ioffe, J. Shlens, and Z. Wojna, “Rethinking the inception architecture for computer vision,” in *CVPR*, 2016.
- [296] H. Zhang, F. Li, S. Liu, L. Zhang, H. Su, J. Zhu, L. M. Ni, and H.-Y. Shum, “Dino: Detr with improved denoising anchor boxes for end-to-end object detection,” in *ICLR*, 2022.
- [297] “<https://github.com/discus0434/aesthetic-predictor-v2-5>,” [Online]. Available: <https://github.com/discus0434/aesthetic-predictor-v2-5>
- [298] N. Silberman, D. Hoiem, P. Kohli, and R. Fergus, “Indoor segmentation and support inference from rgbd images,” in *ECCV*, 2012.
- [299] T. Zhou, R. Tucker, J. Flynn, G. Fyffe, and N. Snavely, “Stereo magnification: Learning view synthesis using multiplane images,” *ACM TOG*, 2018.
- [300] A. Liu, R. Tucker, V. Jampani, A. Makadia, N. Snavely, and A. Kanazawa, “Infinite nature: Perpetual view generation of natural scenes from a single image,” in *ICCV*, 2021.
- [301] C. Schuhmann, R. Beaumont, R. Vencu, C. Gordon, R. Wightman, M. Cherti, T. Coombes, A. Katta, C. Mullis, M. Wortsman *et al.*, “Laion-5b: An open large-scale dataset for training next generation image-text models,” *NeurIPS*, 2022.
- [302] T. Wu, J. Zhang, X. Fu, Y. Wang, J. Ren, L. Pan, W. Wu, L. Yang, J. Wang, C. Qian *et al.*, “Omniobject3d: Large-vocabulary 3d object dataset for realistic perception, reconstruction and generation,” in *CVPR*, 2023.
- [303] Z. Cui, L. Gu, X. Sun, X. Ma, Y. Qiao, and T. Harada, “Aleth-nerf: Illumination adaptive nerf with concealing field assumption,” in *AAAI*, 2024.
- [304] Q. Zuo, X. Gu, Y. Dong, Z. Zhao, W. Yuan, L. Qiu, L. Bo, and Z. Dong, “High-fidelity 3d textured shapes generation by sparse encoding and adversarial decoding,” in *ECCV*, 2024.
- [305] R. Shi, H. Chen, Z. Zhang, M. Liu, C. Xu, X. Wei, L. Chen, C. Zeng, and H. Su, “Zero123++: a single image to consistent multi-view diffusion base model,” *arXiv preprint arXiv:2310.15110*, 2023.
- [306] A. Blattmann, T. Dockhorn, S. Kulal, D. Mendelevitch, M. Kilian, D. Lorenz, Y. Levi, Z. English, V. Voleti, A. Letts *et al.*, “Stable video diffusion: Scaling latent video diffusion models to large datasets,” *arXiv preprint arXiv:2311.15127*, 2023.
- [307] R. Liu, R. Wu, B. Van Hoorick, P. Tokmakov, S. Zakharov, and C. Vondrick, “Zero-1-to-3: Zero-shot one image to 3d object,” in *ICCV*, 2023.
- [308] X. Dai, J. Hou, C.-Y. Ma, S. Tsai, J. Wang, R. Wang, P. Zhang, S. Vandenheide, X. Wang, A. Dubey *et al.*, “Emu: Enhancing image generation models using photogenic needles in a haystack,” *arXiv preprint arXiv:2309.15807*, 2023.
- [309] P. Esser, S. Kulal, A. Blattmann, R. Entezari, J. Müller, H. Saini, Y. Levi, D. Lorenz, A. Sauer, F. Boesel *et al.*, “Scaling rectified flow transformers for high-resolution image synthesis,” in *ICML*, 2024.
- [310] W. Peebles and S. Xie, “Scalable diffusion models with transformers,” in *ICCV*, 2023.
- [311] H. Liu, C. Li, Q. Wu, and Y. J. Lee, “Visual instruction tuning,” *NeurIPS*, 2023.
- [312] K. Huang, K. Sun, E. Xie, Z. Li, and X. Liu, “T2i-compbench: A comprehensive benchmark for open-world compositional text-to-image generation,” *NeurIPS*, 2023.
- [313] J. Wang, K. C. Chan, and C. C. Loy, “Exploring clip for assessing the look and feel of images,” in *AAAI*, 2023.
- [314] H. Wu, Z. Zhang, W. Zhang, C. Chen, L. Liao, C. Li, Y. Gao, A. Wang, E. Zhang, W. Sun, Q. Yan, X. Min, G. Zhai, and W. Lin, “Q-align: Teaching LMMs for visual scoring via discrete text-defined levels,” in *ICML*, 2024.
- [315] S. Jayasumana, S. Ramalingam, A. Veit, D. Glasner, A. Chakrabarti, and S. Kumar, “Rethinking fid: Towards a better evaluation metric for image generation,” in *CVPR*, 2024.
- [316] X. Wu, Y. Hao, K. Sun, Y. Chen, F. Zhu, R. Zhao, and H. Li, “Human preference score v2: A solid benchmark for evaluating human preferences of text-to-image synthesis,” *arXiv:2306.09341*, 2023.
- [317] J. Wang, M. Chen, N. Karaev, A. Vedaldi, C. Rupprecht, and D. Novotny, “Vggt: Visual geometry grounded transformer,” in *CVPR*, 2025.
- [318] S. Zhang, J. Wang, Y. Xu, N. Xue, C. Rupprecht, X. Zhou, Y. Shen, and G. Wetzstein, “Flare: Feed-forward geometry, appearance and camera estimation from uncalibrated sparse views,” in *CVPR*, 2025.